Coulomb Excitation of Double Giant Dipole Resonances

J. Z. Gu and H. A. Weidenmüller

Max-Planck-Institut für Kernphysik, Postfach 103980, D-69029 Heidelberg, Germany

Abstract

We implement the Brink–Axel hypothesis for the excitation of the double giant dipole resonance (DGDR): The background states which couple to the one–phonon giant dipole resonance are themselves capable of dipole absorption. These states (and the ones which couple to the two–phonon resonance) are described in terms of the Gaussian Orthogonal Ensemble of random matrices. We use second–order time–dependent perturbation theory and calculate analytically the ensemble–averaged cross section for excitation of the DGDR. Numerical calculations illuminate the mechanism and the dependence of the cross section on the various parameters of the theory, and are specifically performed for the reaction ^{208}Pb + ^{208}Pb at a projectile energy of 640 MeV/nucleon. We show that the contribution of the background states to the excitation of the DGDR is significant. We find that the width of the DGDR, the energy–integrated cross section and the ratio of this quantity over the energy–integrated cross section for the single giant dipole resonance, all agree with experiment within experimental errors. We compare our approach with that of Carlson *et al.* who have used a similar physical picture.

Keywords: Coulomb excitation, double giant dipole resonance, Gaussian orthogonal ensemble, spreading width

PACS numbers: 24.30.Cz, 25.70.De, 24.60.Ky, 24.60.Lz

e-mail: gu@daniel.mpi-hd.mpg.de

1 Introduction

In peripheral heavy–ion collisions at bombarding energies of several hundred MeV/nucleon and more, the nuclear giant resonances, in particular the isovector giant dipole resonance, are excited by Coulomb excitation. Recently, the excitation of higher dipole modes – the multi–phonon excitation – has attracted particular attention.

In the simplest and idealized picture, the giant dipole resonance (GDR) is a one–phonon state described by the collective motion of all protons against all neutrons. In addition, there exist also higher vibrational modes (many–phonon states) that can be excited by multi–photon absorption. In the harmonic oscillator approximation, the excitation energy of the n–phonon resonance is exactly equal to n times that of the GDR, and its width is equal to n times the width of the GDR provided the strength distribution is approximated by a Lorentzian.

The double giant dipole resonance (DGDR) has been observed in several nuclei: ^{136}Xe [1], ^{197}Au [2] and ^{208} Pb [3, 4]. Compared to the predictions of the harmonic picture, the measured cross sections for the DGDR excitation are found to be enhanced by factors ranging from 1.3 to 2 [5, 6, 7]. At the same time the experimentally determined widths of the DGDR are close to $\sqrt{2}$ times the width of the GDR. These discrepancies between simple–minded theoretical predictions and experimental results have attracted much theoretical attention. Several mechanisms have been studied. We mention anharmonicities of the collective Hamiltonian [8, 9] and nonlinearities of the external field [10]. Following several earlier papers, Carlson *et al.* [11, 12] have recently discussed the discrepancy using the Brink–Axel hypothesis. This hypothesis states that a giant resonance is built on top of *every* excited nuclear state [13]. Following work by Ko [14], these authors considered the contribution to the cross section of DGDR excitation due to the background states which couple dynamically to the one–phonon state. It was found that this contribution is sizable.

This result is interesting and calls for further study, especially since the approach of Carlson *et al.* [11, 12] uses approximations which are plausible but not based upon an expansion in terms of a small parameter, see Section 6. In the present paper, we apply essentially the same physical picture as Carlson *et al.* but use a formulation which allows us to derive the DGDR excitation cross section within perfectly controlled approximations. The resulting formula is subsequently evaluated numerically. Our approach makes it possible to clearly identify and calculate the modification of the DGDR absorption process due to the Brink–Axel hypothesis.

The paper is organized as follows. We describe our approach in Section 2. The background

states which couple to the collective one– and two–phonon states are complex states. These states are, therefore, modeled with the help of random–matrix theory [15, 16]. In Section 3, we derive the expression for the cross section for DGDR excitation in the framework of second–order time–dependent perturbation theory. The specific way in which the Brink–Axel hypothesis has been implemented allows for a substantial simplification of the resulting expressions (Section 3.2). An analytical expression for the ensemble–averaged cross section is derived in Section 4. In Section 5, numerical calculations are used to illuminate our results and are specifically performed for the reaction ^{208}Pb + ^{208}Pb at projectile energy 640 MeV/nucleon [7]. We calculate the width of the DGDR, the energy–integated cross section, and the ratio of this quantity over the energy–integrated cross section for single dipole absorption. In Section 6, we compare our approach and that of Carlson *et al.* A brief summary is given in Section 7.

2 Hamiltonian of the Projectile

We consider the relativistic Coulomb excitation of the DGDR of the projectile in a collision with a target.

For the Hamiltonian of the projectile, we use the physical picture shown in Fig. 1. In the random–phase approximation (RPA), the one–phonon and the two–phonon states of the projectile are coherent superpositions of one–particle one–hole (1p1h) states and of two–particle two–hole (2p2h) states, respectively. The one–phonon state $|10\rangle$ is the giant dipole mode of the ground state $|00\rangle$, and the two–phonon state $|20\rangle$ is the giant dipole mode of the one–phonon state. The one–phonon state $|10\rangle$ is dynamically coupled by the nuclear Hamiltonian to more complex particle–hole configurations $|0k\rangle$ with $k = 1, \ldots, K$ and $K \gg 1$. This coupling causes the giant dipole resonance to acquire a spreading width $\Gamma_{10}^{\downarrow}$. The two–phonon state $|20\rangle$ is likewise coupled to such configurations. In order to accommodate the Brink–Axel hypothesis, we group these configurations into two classes. States in the first class are denoted by $|1k\rangle$ with $k = 1, \ldots, K$. Each such state represents the dipole mode of the lower state $|0k\rangle$. States in the second class are denoted by $|0\alpha\rangle$ with $\alpha = 1, \ldots, M$ and $M \gg 1$. These latter states are not coupled by the dipole operator to lower–lying configurations. The states $|20\rangle$, $|1k\rangle$ and $|0\alpha\rangle$ are all dynamically coupled to each other.

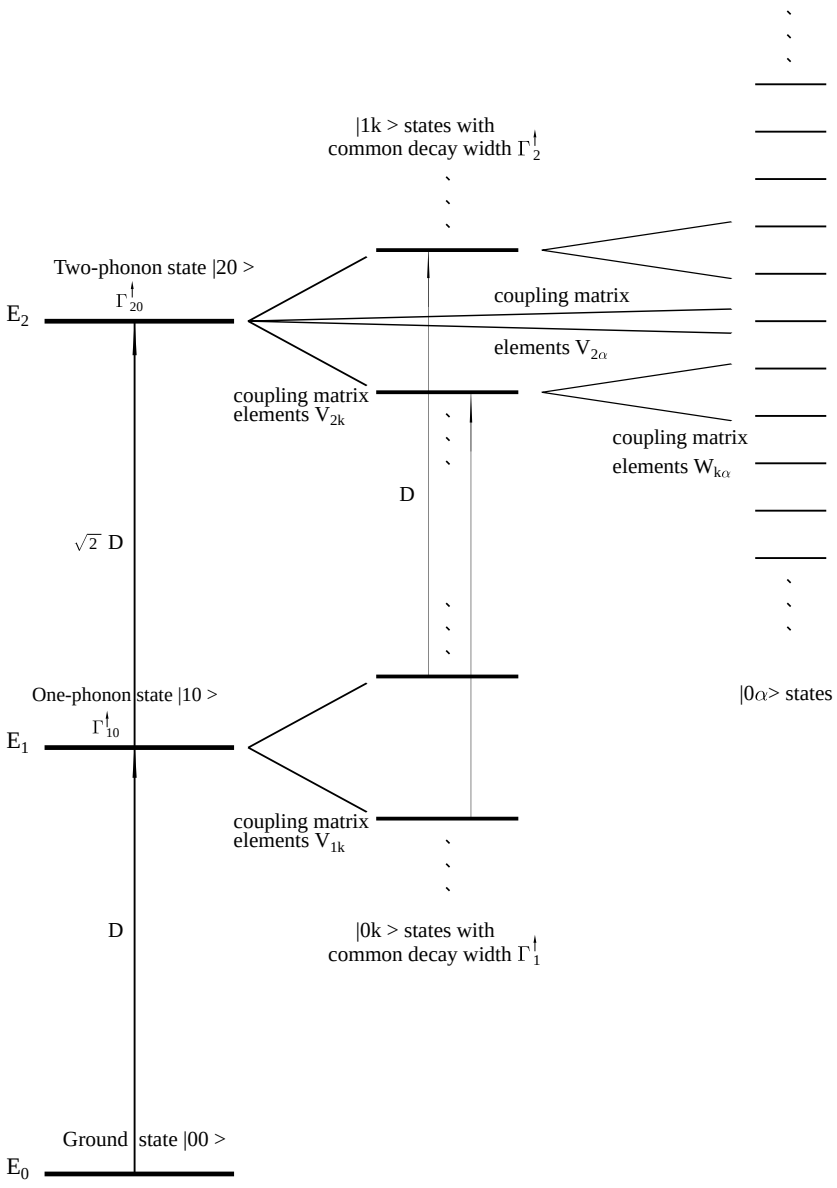

Figure 1: Schematic illustration of the DGDR excitation and the couplings between the phonon states and many-particle many-hole configurations. The level spacings of the configurations are exaggerated in the figure.

According to this picture, the Hamiltonian matrix H has the form

$$H = \begin{pmatrix} E_0 & \emptyset & \emptyset & \emptyset & \emptyset & \emptyset \\ \emptyset & E_1 & V_{1k} & \emptyset & \emptyset & \emptyset \\ \emptyset & V_{l1} & H^{(0)}_{lk} & \emptyset & \emptyset & \emptyset \\ \emptyset & \emptyset & \emptyset & E_2 & V_{2k'} & V_{2\alpha} \\ \emptyset & \emptyset & \emptyset & V_{l'2} & H^{(1)}_{l'k'} & W_{l'\alpha} \\ \emptyset & \emptyset & \emptyset & V_{\beta 2} & W_{\beta k'} & \mathcal{H}^{(0)}_{\beta\alpha} \end{pmatrix} . \tag{1}$$

The matrix H consists of three diagonal blocks. The first block has dimension one and contains the energy E_0 of the ground state $|00\rangle$. The second block has dimension $1+K$. It contains the unperturbed energy E_1 of the one–phonon state $|10\rangle$, the elements $H^{(0)}_{kl}$ with $k,l = 1,\ldots,K$ of the Hamiltonian matrix $H^{(0)}$ governing the states $|0k\rangle$, and the real coupling matrix elements V_{1k} connecting the one–phonon state with the states $|0k\rangle$. The third block has dimension $1+K+M$. It contains the unperturbed energy E_2 of the two–phonon state $|20\rangle$, the Hamiltonian matrices $H^{(1)}_{kl}$ with $k,l = 1,\ldots,K$ and $\mathcal{H}^{(0)}_{\alpha\beta}$ with $\alpha,\beta = 1,\ldots,M$ governing the states $|1k\rangle$ and $|0\alpha\rangle$, respectively, and the real coupling matrix elements V_{2k}, $V_{2\alpha}$ and $W_{k\alpha}$ connecting the three sets of states. In this simple picture, we pay no attention to spin and isospin. Inclusion of these quantum numbers is not difficult but requires a straightforward extension of our formalism. If, for instance, the ground state has spin and parity 0^+, then all states in block two have spin and parity 1^-, while the states in block three decay into three groups having spin/parity values $0^+, 1^+$ and 2^+, respectively.

We turn to the statistical assumptions. We describe the K states $|0k\rangle$ with $K \to \infty$ in terms of the Gaussian Orthogonal Ensemble of random matrices (GOE), so that $H^{(0)}$ represents this ensemble. For excitation energies of the giant dipole resonance (which lie typically between 8 and 15 MeV), this description seems eminently reasonable, except perhaps for the lightest nuclei. The spreading width $\Gamma^{\downarrow}_{10} = 2\pi v^2/d$ of the giant dipole resonance is expressed in terms of the mean level spacing d of the states $|0k\rangle$ and of the mean square coupling matrix element $\overline{V^2_{1k}} = v^2$. It was mentioned above that for each value of $k = 1,\ldots,K$, the state $|1k\rangle$ is assumed to be the giant dipole mode of the state $|0k\rangle$. This implies that the matrix $H^{(1)}$ is identical to $H^{(0)}$ except that the center of the semicircle is shifted by $E_2 - E_1$, so that

$$H^{(1)}_{kl} = (E_2 - E_1)\delta_{kl} + H^{(0)}_{kl} \ . \tag{2}$$

We also assume that $V_{1k} = V_{2k}$. This assumption is not strictly implied by the Brink–Axel hypothesis because the states $|10\rangle$ and $|20\rangle$ (or $|0k\rangle$ and $|1k\rangle$, respectively) are not identical.

Rather, we have $|20\rangle \propto D|10\rangle$ where D is the dipole operator, and correspondingly for the states labelled k. In practice, the assumption $V_{1k} = V_{2k}$ implies that the spreading widths for the couplings $|10\rangle \Leftrightarrow |0k\rangle$ and $|20\rangle \Leftrightarrow |1k\rangle$ are equal. This assumption seems plausible. We return to this point in Section 5. We note that with these assumptions, the second block of the matrix (1) differs from the corresponding part of the third block only by $(E_2 - E_1)$ times the unit matrix. The matrix $\mathcal{H}^{(0)}$ is also assumed to represent a GOE, with M taken to infinity. We assume that $\mathcal{H}^{(0)}$ and $H^{(0)}$ are uncorrelated.

The states in the second and third block can decay by particle emission. We take account of this fact by introducing the decay widths $\Gamma^{\uparrow}_{10}$ and $\Gamma^{\uparrow}_{20}$ of the one–phonon and the two–phonon states, respectively, and the decay widths $\Gamma^{\uparrow}_{1}$ and $\Gamma^{\uparrow}_{2}$ of the states $|0k\rangle$ and $|1k\rangle$, respectively. Within the statistical model, it is obviously adequate to assume that $\Gamma^{\uparrow}_{1}$ and $\Gamma^{\uparrow}_{2}$ are independent of the running index $k = 1, \ldots, K$. In Section 3.2 it is shown that it is not necessary to assign a decay width to the states $|0\alpha\rangle$. The width matrix Σ accordingly has the form

$$\Sigma = -(i/2) \begin{pmatrix} 0 & 0 & 0 & 0 & 0 & 0 \\ 0 & \Gamma^{\uparrow}_{10} & 0 & 0 & 0 & 0 \\ 0 & 0 & \delta_{lk}\Gamma^{\uparrow}_{1} & 0 & 0 & 0 \\ 0 & 0 & 0 & \Gamma^{\uparrow}_{20} & 0 & 0 \\ 0 & 0 & 0 & 0 & \delta_{l'k'}\Gamma^{\uparrow}_{2} & 0 \\ 0 & 0 & 0 & 0 & 0 & 0 \end{pmatrix} . \tag{3}$$

The effective Hamiltonian H_{eff} is then given by

$$H_{\text{eff}} = H + \Sigma \ . \tag{4}$$

All four decay widths can be calculated with the help of the optical model. We return to this point in Section 5.

3 Second–order Time–dependent Perturbation Theory

We suppress the intrinsic structure of the target and replace it by a point source of the electromagnetic field. To describe the DGDR excitation of the projectile, we use the standard approach to Coulomb excitation [17]: The relative motion of projectile and target is described classically, and the intrinsic excitation of the projectile is treated quantum–mechanically.

3.1 General Approach

The time–dependent Schrödinger equation

$$i\hbar\frac{\partial|\psi(t)\rangle}{\partial\, t} = (H_{\rm eff} + H_1(t))|\psi(t)\rangle \tag{5}$$

for the internal wave function $|\psi(t)\rangle$ of the projectile contains the interaction $H_1(t)$ with the time–dependent electromagnetic field caused by the relative motion. We consider only dipole excitation and write $H_1(t) = Dh(t)$ as the product of the dipole operator D and of a time–dependent function $h(t)$. We have $h(t) \to 0$ for $t \to \pm\infty$. A suitable form for $h(t)$ is given in Section 5. The dipole operator D induces transitions between the following pairs of states: $|00\rangle \to |10\rangle$, $|10\rangle \to |20\rangle$, and $|0k\rangle \to |1k\rangle$ for all $k = 1, \ldots, K$.

We use the interaction representation

$$|\phi(t)\rangle = \exp(iH_{\rm eff}\, t/\hbar)|\psi(t)\rangle \tag{6}$$

so that

$$i\hbar\frac{\partial|\phi(t)\rangle}{\partial\, t} = \widetilde{H}_1(t)|\phi(t)\rangle \tag{7}$$

with

$$\widetilde{H}_1(t) = \exp(iH_{\rm eff}\, t/\hbar)H_1(t)\exp(-iH_{\rm eff}\, t/\hbar)\ . \tag{8}$$

Excitation of the DGDR is a two–step process. We use second–order time–dependent perturbation theory. With $|\phi(-\infty)\rangle = |00\rangle$ and $\widetilde{H}_1(t) \to\ 0$ for $t \to \pm\infty$, we have

$$|\phi(+\infty)\rangle = (\frac{1}{i\hbar})^2 \int_{-\infty}^{\infty} dt_1 \widetilde{H}_1(t_1) \int_{-\infty}^{t_1} dt_2 \widetilde{H}_1(t_2)|00\rangle\ . \tag{9}$$

To calculate the intensity I_2 for double dipole excitation with energy transfer E', we first consider the case where $\Gamma_{20}^{\uparrow}$ and $\Gamma_{2}^{\uparrow}$ both vanish. Let $|n\rangle$ represent an eigenstate with energy E_n of the submatrix $H_{\rm eff,33}$ forming the third block of the matrix $H_{\rm eff}$. Then I_2 is given by

$$I_2(E' + E_0) = \sum_n |\langle\, n|\phi(+\infty)\rangle|^2 \delta(E' - (E_n - E_0))\ . \tag{10}$$

For I_2 we have used the argument $E' + E_0$ rather than E' because it is convenient to introduce $E = E' + E_0$. Moreover, we use the identity

$$\sum_n |n\rangle\langle\, n|\delta(E - E_n) = \frac{(-)}{\pi}{\rm Im}\frac{1}{E^+ - H_{\rm eff,33}}\ , \tag{11}$$

the definition of $\widetilde{H_1}(t)$ given above, and the fact that $H_{\rm eff}|00\rangle = E_0|00\rangle$ to rewrite $I_2(E)$ in the form

$$I_2(E) = -\frac{1}{\pi\,\hbar^4}\int_{-\infty}^{\infty} dt_1 \int_{-\infty}^{t_1} dt_2 \int_{-\infty}^{\infty} dt_1' \int_{-\infty}^{t_1'} dt_2' \langle 00|H_1^*(t_2')\exp\{-i(H_{\rm eff}^* - E_0)(t_2'-t_1')/\hbar\}$$
$$\times H_1^*(t_1')\exp\{-i(H_{\rm eff}^* - E_0)t_1'/\hbar\}{\rm Im}(\frac{1}{E^+ - H_{\rm eff,33}})\exp\{i(H_{\rm eff}-E_0)t_1/\hbar\}$$
$$\times H_1(t_1)\exp\{i(H_{\rm eff}-E_0)(t_2-t_1)/\hbar\}H_1(t_2)|00\rangle\ . \qquad (12)$$

The form of Eq. (12) remains unchanged when we take account of the finite values of the decay widths $\Gamma_{20}^{\uparrow}$ and $\Gamma_2^{\uparrow}$. Substitution of $H_1(t) = Dh(t)$ yields

$$I_2(E) = -\frac{1}{\pi\,\hbar^4}\int_{-\infty}^{\infty} dt_1 \int_{-\infty}^{0} d\tau_2 \int_{-\infty}^{\infty} dt_1' \int_{-\infty}^{0} d\tau_2'\, h(t_1)h(\tau_2+t_1)h^*(t_1')h^*(\tau_2'+t_1')$$
$$\times\langle 00|D\exp\{-i(H_{\rm eff,22}^* - E_0)\tau_2'/\hbar\}D\exp\{i(E-E_0)(t_1-t_1')/\hbar\}$$
$$\times{\rm Im}(\frac{1}{E^+ - H_{\rm eff,33}})D\exp\{i(H_{\rm eff,22}-E_0)\tau_2/\hbar\}D|00\rangle, \qquad (13)$$

with $\tau_2 = t_2 - t_1$ and $\tau_2' = t_2' - t_1'$. We have replaced $\exp\{i(H_{\rm eff,33}-E_0)(t_1-t_1')/\hbar\}$ by $\exp\{i(E-E_0)(t_1-t_1')/\hbar\}$. The remaining two exponentials in Eq. (13) contain the second block $H_{\rm eff,22}$ of $H_{\rm eff}$ and can be expressed in terms of Green functions. The integrand of

$$\int_{-\infty}^{\infty} d\epsilon \frac{1}{\epsilon^+ - H_{\rm eff}}\exp(-i\epsilon\ t/\hbar) \qquad (14)$$

has poles in the lower half of the ϵ plane. We may close the contour of integration in the upper (lower) half plane if $t<0$ ($t>0$, respectively). Hence,

$$\int_{-\infty}^{\infty} d\epsilon \frac{1}{\epsilon^+ - H_{\rm eff}}\exp(i\epsilon\ t/\hbar) = -2i\pi\Theta(-t)\exp(iH_{\rm eff}t/\hbar)\ , \qquad (15)$$

$$\int_{-\infty}^{\infty} d\epsilon \frac{1}{\epsilon^- - H_{\rm eff}}\exp(-i\epsilon\ t/\hbar) = 2i\pi\Theta(-t)\exp(-iH_{\rm eff}t/\hbar)\ . \qquad (16)$$

We observe that both the τ_2–integration and the τ_2'–integration are restricted to values ≤ 0. We use the formulas (15) and (16) to find

$$I_2(E)\ = -\ (\frac{1}{\pi\,\hbar^4})\ \int_{-\infty}^{\infty} dt_1 \int_{-\infty}^{0} d\tau_2 \int_{-\infty}^{\infty} dt_1' \int_{-\infty}^{0} d\tau_2'\ h(t_1)\ h(\tau_2+t_1)\ h^*(t_1')\ h^*(\tau_2'+t_1')$$
$$\times\exp\{i(E-E_0)(t_1-t_1')/\hbar\}\int_{-\infty}^{\infty} d\epsilon \int_{-\infty}^{\infty} d\epsilon' \exp\{i(\epsilon-E_0)\tau_2/\hbar\}\exp\{-i(\epsilon'-E_0)\tau_2'/\hbar\}$$
$$\times M(E,\epsilon,\epsilon')\ . \qquad (17)$$

Here, M is a stochastic function of $H_{\rm eff}$ defined by

$$M(E,\epsilon,\epsilon') = \langle 00|D\frac{1}{(\epsilon')^- - H_{\rm eff,22}^*}D{\rm Im}(\frac{1}{E^+ - H_{\rm eff,33}})D\frac{1}{\epsilon^+ - H_{\rm eff,22}}D|00\rangle\ . \qquad (18)$$

To simplify M, we observe that D does not connect to the rows and columns labelled α and β in the third block of the matrix in Eq. (1). Therefore, we restrict attention in the third block to the subspace of states obtained by excluding these rows and columns. The projection of $H_{\rm eff,33}$ onto this subspace (which we denote by s) is written as $H_{{\rm eff},s}$, and we have

$$[\frac{1}{E-H_{\rm eff,33}}]_s = \frac{1}{E-H_{{\rm eff},s}-W'\frac{1}{E^+-\mathcal{H}^{(0)}}(W')^\dagger} \ , \tag{19}$$

where $W' = (V_{2\alpha}, W_{l'\alpha})$. We insert this result back into Eq. (18) and find

$$M(E,\epsilon,\epsilon') = \langle 00|D\frac{1}{\epsilon'-H^*_{\rm eff,22}}D{\rm Im}(\frac{1}{E-H_{{\rm eff},s}-W'\frac{1}{E^+-\mathcal{H}^{(0)}}(W')^\dagger})D\frac{1}{\epsilon-H_{\rm eff,22}}D|00\rangle \ . \tag{20}$$

Eqs. (17) and (20) are the central results of this Section.

3.2 Simplification of M

The expression for M can be simplified further because $H^{(0)}$ and $\mathcal{H}^{(0)}$ are uncorrelated. Since $\mathcal{H}^{(0)}$ appears in the intensity $I_2(E)$ only via the expression (20), we can perform the average over $\mathcal{H}^{(0)}$ right away. We have

$$\overline{W'\frac{1}{E^+-\mathcal{H}^{(0)}}(W')^\dagger} = -\Sigma_s^\downarrow = -(i/2)\begin{pmatrix} \Gamma_{20}^\downarrow & 0 \\ 0 & \delta_{l'k'}\Gamma_2^\downarrow \end{pmatrix} \ . \tag{21}$$

Here $\Gamma_{20}^\downarrow$ is the spreading width of the two–phonon state due to its coupling to the states $|0\alpha\rangle$, and $\Gamma_2^\downarrow$ is the common spreading width of the states $|1k\rangle$ due to their coupling to the states $|0\alpha\rangle$. We observe that the result of the averaging procedure is independent of whether or not we include a decay width for the states $|0\alpha\rangle$, see the end of Section 2. We use the result of Eq. (21) in Eq. (20). To justify this step, we observe that a series expansion of the right–hand side of Eq. (20) in powers of the Green function of $\mathcal{H}^{(0)}$, followed by averaging over $\mathcal{H}^{(0)}$, would amount to taking the average individually over each Green function appearing in the expansion. This is because the energy argument in all these functions has a positive imaginary part. Resummation of the result amounts to using the result of Eq. (21) in Eq. (20). This yields for M

$$M(E,\epsilon,\epsilon') = \langle 00|D\frac{1}{\epsilon'-H^*_{\rm eff,22}}D{\rm Im}(\frac{1}{E-H_{{\rm eff},s}+\Sigma_s^\downarrow})D\frac{1}{\epsilon-H_{\rm eff,22}}D|00\rangle \ . \tag{22}$$

A further simplification of M is possible because the real part of $H_{{\rm eff},s}$ differs from the real part of $H_{\rm eff,22}$ only by (E_2-E_1) times the unit matrix, see Eq. (2). To use this fact, it is necessary

to write the matrices appearing in the three Green functions in Eq. (22) more explicitly. We denote the real part of $H_{\mathrm{eff},22}$ by H_{22} and have

$$H_{22} = \begin{pmatrix} E_1 & V_{1k} \\ V_{l1} & H^{(0)}_{lk} \end{pmatrix} \ . \tag{23}$$

Moreover, we define

$$\Sigma_1 = (i/2) \begin{pmatrix} \Gamma^{\uparrow}_{10} & 0 \\ 0 & \delta_{jl}\Gamma^{\uparrow}_1 \end{pmatrix} \ , \tag{24}$$

and, with $\widetilde{\Gamma_{20}} = \Gamma^{\uparrow}_{20} + \Gamma^{\downarrow}_{20}$, $\Gamma_2 = \Gamma^{\uparrow}_2 + \Gamma^{\downarrow}_2$,

$$\Sigma_2 = (i/2) \begin{pmatrix} \widetilde{\Gamma_{20}} & 0 \\ 0 & \delta_{jl}\Gamma_2 \end{pmatrix} \ . \tag{25}$$

Then, M takes the form

$$M(E,\epsilon,\epsilon') = \langle 00|D\frac{1}{\epsilon' - H_{22} - \Sigma_1}D\mathrm{Im}(\frac{1}{E - E_2 + E_1 - H_{22} + \Sigma_2})D\frac{1}{\epsilon - H_{22} + \Sigma_1}D|00\rangle \ . \tag{26}$$

A further simplification of this expression is possible with the help of the Brink–Axel hypothesis and of algebraic identities. In the spirit of the Brink–Axel hypothesis, we assume that the dipole transitions $|00\rangle \to |10\rangle$ and $|0k\rangle \to |1k\rangle$ all have identical dipole matrix elements. We denote all these identical matrix elements also by D. We also take account of the fact that in the harmonic oscillator picture, the dipole matrix element for the transition $|10\rangle \to |20\rangle$ is given by $\sqrt{2}D$. Using these facts, we can express M completely in terms of the Green functions

$$\begin{aligned} G^{\pm}_1(E) &= \langle 10|\frac{1}{E - H_{22} \pm \Sigma_1}|10\rangle \ , \\ G^{\pm}_2(E) &= \langle 10|\frac{1}{E - H_{22} \pm \Sigma_2}|10\rangle \ . \end{aligned} \tag{27}$$

To this end, we introduce the $(1+K)$–dimensional unit matrix $\mathcal{I}$, define $\delta\sigma, \delta\sigma_0, \delta\tau, \delta\tau_0, \delta\rho$ and $\delta\rho_0$ by

$$\Sigma_2 - \Sigma_1 = \delta\sigma\, \mathcal{I} + \delta\sigma_0\ |10\rangle\langle 10|, \tag{28}$$

$$\Sigma_2 + \Sigma_1 = \delta\tau\, \mathcal{I} + \delta\tau_0\ |10\rangle\langle 10|, \tag{29}$$

$$2\ \Sigma_1 = \delta\rho\, \mathcal{I} + \delta\rho_0\ |10\rangle\langle 10| \ , \tag{30}$$

and make use of the identities

$$\begin{aligned} \frac{1}{E - H_{22} + \Sigma_2}\ \frac{1}{\epsilon - H_{22} + \Sigma_1} &= \frac{1}{E - \epsilon + \delta\sigma}(\frac{1}{\epsilon - H_{22} + \Sigma_1} - \frac{1}{E - H_{22} + \Sigma_2}) \\ -\frac{\delta\sigma_0}{E - \epsilon + \delta\sigma}\ \frac{1}{E - H_{22} + \Sigma_2}&|10\rangle\langle 10|\frac{1}{\epsilon - H_{22} + \Sigma_1}, \end{aligned} \tag{31}$$

$$\frac{1}{E-H_{22}+\Sigma_2}\ \frac{1}{\epsilon'-H_{22}-\Sigma_1}=\frac{1}{E-\epsilon'+\delta\tau}(\frac{1}{\epsilon'-H_{22}-\Sigma_1}-\frac{1}{E-H_{22}+\Sigma_2})$$
$$-\frac{\delta\tau_0}{E-\epsilon'+\delta\tau}\ \frac{1}{E-H_{22}+\Sigma_2}|10\rangle\langle 10|\frac{1}{\epsilon'-H_{22}-\Sigma_1}\ , \tag{32}$$

$$\frac{1}{\epsilon'-H_{22}-\Sigma_1}\ \frac{1}{\epsilon-H_{22}+\Sigma_1}=\frac{1}{\epsilon-\epsilon'+\delta\rho}(\frac{1}{\epsilon'-H_{22}-\Sigma_1}-\frac{1}{\epsilon-H_{22}+\Sigma_1})$$
$$-\frac{\delta\rho_0}{\epsilon-\epsilon'+\delta\rho}\ \frac{1}{\epsilon'-H_{22}-\Sigma_1}|10\rangle\langle 10|\frac{1}{\epsilon-H_{22}+\Sigma_1}\ . \tag{33}$$

We define $E''=E-E_2+E_1$ and obtain as a result

$$M(E,\epsilon,\epsilon')=\frac{i}{2}D^4\ \Big(\frac{G_1^-(\epsilon')}{\epsilon-\epsilon'+\delta\rho}(\frac{1}{E''-\epsilon'-\delta\sigma}-\frac{1}{E''-\epsilon'+\delta\tau})$$
$$+\frac{G_1^+(\epsilon)}{\epsilon-\epsilon'+\delta\rho}(\frac{1}{E''-\epsilon+\delta\sigma}-\frac{1}{E''-\epsilon-\delta\tau})$$
$$+(\frac{1}{E''-\epsilon-\delta\tau}\ \frac{1}{E''-\epsilon'-\delta\sigma}G_2^-(E'')-\frac{1}{E''-\epsilon+\delta\sigma}\ \frac{1}{E''-\epsilon'+\delta\tau}\ G_2^+(E''))$$
$$+G_1^-(\epsilon')G_1^+(\epsilon)[(\frac{1}{E''-\epsilon'-\delta\tau}-\frac{1}{E''-\epsilon'+\delta\tau})(\frac{\delta\sigma_0}{\epsilon-\epsilon'+\delta\rho}+\sqrt{2}-1)$$
$$+(\frac{1}{E''-\epsilon'+\delta\sigma}-\frac{1}{E''-\epsilon'-\delta\sigma})(\frac{\delta\tau_0}{\epsilon-\epsilon'+\delta\rho}+1-\sqrt{2})]$$
$$-(\frac{\delta\tau_0}{E''-\epsilon-\delta\tau}+\sqrt{2}-1)\ \frac{G_2^-(E'')G_1^+(\epsilon)}{E''-\epsilon'-\delta\sigma}-(\frac{\delta\tau_0}{E''-\epsilon'+\delta\tau}+1-\sqrt{2})\ \frac{G_1^-(\epsilon')G_2^+(E'')}{E''-\epsilon+\delta\sigma}$$
$$-(\frac{\delta\sigma_0}{E''-\epsilon'-\delta\sigma}+\sqrt{2}-1)\ \frac{G_2^-(E'')G_1^-(\epsilon')}{E''-\epsilon'-\delta\tau}-(\frac{\delta\sigma_0}{E''-\epsilon+\delta\sigma}+1-\sqrt{2})\ \frac{G_1^+(\epsilon)G_2^+(E'')}{E''-\epsilon+\delta\tau}$$
$$+G_1^-(\epsilon')G_1^+(\epsilon)\ \{G_2^-(E'')[\frac{\delta\tau_0\delta\sigma_0}{(E''-\epsilon-\delta\tau)\ (E''-\epsilon'-\delta\sigma)}$$
$$+(\sqrt{2}-1)(\frac{\delta\tau_0}{E''-\epsilon-\delta\tau}+\frac{\delta\sigma_0}{E''-\epsilon'-\delta\sigma})+3-2\sqrt{2}]$$
$$+G_2^+(E'')[-\frac{\delta\tau_0\delta\sigma_0}{(E''-\epsilon+\delta\sigma)\ (E''-\epsilon'+\delta\tau)}$$
$$+(\sqrt{2}-1)(\frac{\delta\sigma_0}{E''-\epsilon+\delta\sigma}+\frac{\delta\tau_0}{E''-\epsilon'+\delta\tau})+2\sqrt{2}-3]\}\Big). \tag{34}$$

Terms carrying the factor $(\sqrt{2}-1)$ arise because not all dipole matrix elements are equal to D. We note that the stochastic matrix H_{22} appears in Eq. (34) only in the Green functions $G_1^{\pm}$ and $G_2^{\pm}$.

4 Ensemble Average and Energy Integration

The ensemble average over $H^{(0)}$ affects only the Green functions $G_1^{\pm}$ and $G_2^{\pm}$ in Eq. (34). The terms in the first three lines of Eq. (34) contain a single Green function (a "one–point function")

only. The next four lines contain products of two Green functions of the type G^+G^- (a "two–point function"), and the last four lines contain two three–point functions. Calculating the ensemble average of the one–point functions is straightforward, see Eq. (21), and yields

$$\overline{G_1^{\pm}(\epsilon)} = \frac{1}{\epsilon - E_1 \pm \frac{i}{2}\Gamma_{10}} \ , \tag{35}$$

$$\overline{G_2^{\pm}(E)} = \frac{1}{E - E_1 \pm \frac{i}{2}\Gamma_{20}} \ . \tag{36}$$

Here $\Gamma_{10} = \Gamma_{10}^{\uparrow} + \Gamma_{10}^{\downarrow}$ and $\Gamma_{20} = \widetilde{\Gamma_{20}} + \Gamma_{10}^{\downarrow}$.

We turn to the ensemble average of the two–point functions. These are written as the sum of two terms, the product of the averages of the two Green functions and the average over the product of the fluctuating parts δG. For example, $\overline{G_1^+(\epsilon)G_2^-(E'')} = \overline{G_1^+(\epsilon)}\ \overline{G_2^-(E'')} + \overline{\delta G_1^+(\epsilon)\delta G_2^-(E'')}$. The last term can be calculated with the help of the supersymmetry technique [18, 19]. We do not give the details here because application of the technique shows that these terms are negligible. This is because the decay widths $\Gamma_{10}^{\uparrow}, \Gamma_1^{\uparrow}, \Gamma_{20}^{\uparrow}, \Gamma_2^{\uparrow}$ turn out to be orders of magnitude larger than the mean level spacing d of the states $|0k\rangle$, see Section 5. This fact leads to an exponential suppression of the fluctuating part. As a result we have, to a very good approximation,

$$\overline{G_1^+(\epsilon)\ G_2^-(E'')} = \overline{G_1^+(\epsilon)}\ \ \overline{G_2^-(E'')} \ . \tag{37}$$

We have already remarked that the average of the product of two retarded Green functions (or of two advanced Green functions) is trivially equal to the product of the averages. Thus, we find that the averages over all two–point functions in Eq. (34) are equal to the product of the averages of the two Green functions. We turn to the average over the three–point functions. Here, a similar argument is expected to apply. Unfortunately, the supersymmetry technique is not capable of giving an analytical result in this case, and we have used numerical simulations to estimate the fluctuating part. For the nucleus ^{208}Pb, for instance, we have found that the contribution of the fluctuating part is less than one part in 10^4. Hence, we have

$$\overline{G_1^+G_1^-G_2^{\pm}} \cong \overline{G_1^+G_1^-}\ \ \overline{G_2^{\pm}} = \overline{G_1^+}\ \ \overline{G_1^-}\ \ \overline{G_2^{\pm}} \ , \tag{38}$$

and the ensemble average of $M(E, \epsilon, \epsilon')$ and $I_2(E)$ can be computed in terms of the ensemble–averaged one–point functions.

4.1 Total Intensity

Using contour integration, we calculate the integrals over the variables ϵ and ϵ'. This calculation is lengthy but straightforward. Using Eq. (34), we find

$$
\begin{aligned}
\overline{I_2(E)} = 2\pi\, i(\frac{D}{\hbar})^4 \int_{-\infty}^{+\infty} dt_1 \int_{-\infty}^{0} d\tau_2 \int_{-\infty}^{+\infty} dt_1' \int_{-\infty}^{0} d\tau_2' \\
h(t_1)h(t_1+\tau_2)h^*(t_1')h^*(t_1'+\tau_2')\exp[i(E-E_0)(t_1-t_1')/\hbar] \\
\times\Big(f_0\Theta(\tau_2-\tau_2')\exp[-i(E_1-E_0+\frac{i}{2}\Gamma_{10})\tau_2'/\hbar]\exp[i(E_1-E_0+\frac{i}{2}\Gamma_{10}-i\Delta\rho)\tau_2/\hbar] \\
\quad\times(f_1^+(E)-f_2^-(E)) \\
+f_0\Theta(\tau_2-\tau_2')\exp[-i(E''-E_0+i\Delta\tau)\tau_2'/\hbar]\exp[i(E''-E_0+i\Delta\sigma)\tau_2/\hbar](f_2^+(E)-f_1^+(E)) \\
-f_0\Theta(\tau_2'-\tau_2)\exp[-i(E''-E_0-i\Delta\sigma)\tau_2'/\hbar]\exp[i(E''-E_0-i\Delta\tau)\tau_2/\hbar](f_2^-(E)-f_1^-(E)) \\
-f_0\Theta(\tau_2'-\tau_2)\exp[-i(E_1-E_0-\frac{i}{2}\Gamma_{10}+i\Delta\rho)\tau_2'/\hbar]\exp[i(E_1-E_0-\frac{i}{2}\Gamma_{10})\tau_2/\hbar] \\
\quad\times(f_1^-(E)-f_2^+(E)) \\
+(\sqrt{2}-1+i\Delta\sigma_0 f_2^-(E))(-\overline{G_2^-(E'')} \\
+(1+i\Delta\tau_0\overline{G_2^-(E'')})f_1^-(E))\exp[-i(E_1-E_0+\frac{i}{2}\Gamma_{10})\tau_2'/\hbar]\exp[i(E''-E_0-i\Delta\tau)\tau_2/\hbar] \\
+(1-\sqrt{2}+i\Delta\sigma_0 f_2^+(E))(-\overline{G_2^+(E'')} \\
+(1-i\Delta\tau_0\overline{G_2^+(E'')})f_1^+(E))\exp[-i(E''-E_0+\Delta\tau)\tau_2'/\hbar]\exp[i(E_1-E_0-\frac{i}{2}\Gamma_{10})\tau_2/\hbar] \\
-[(1-\sqrt{2}+i\Delta\sigma_0\ f_2^+(E))(1-i\Delta\tau_0\overline{G_2^+(E'')})f_1^+(E) \\
+(\sqrt{2}-1+i\Delta\sigma_0\ f_2^-(E))(1+i\Delta\tau_0\overline{G_2^-(E'')})f_1^-(E)) \\
+\Delta\rho_0\frac{1}{\Gamma_{10}-\Delta\rho}(f_2^-(E)-f_2^+(E))+(\sqrt{2}-1)(\overline{G_2^-(E'')}-\overline{G_2^+(E'')})] \\
\quad\times\exp[-i(E_1-E_0+\frac{i}{2}\Gamma_{10})\tau_2'/\hbar]\exp[i(E_1-E_0-\frac{i}{2}\Gamma_{10})\tau_2/\hbar]\Big)\ , \qquad (39)
\end{aligned}
$$

with

$$
\begin{aligned}
f_1^{\pm}(E) &= \frac{1}{E-E_2\mp\frac{i}{2}\Gamma_{10}\pm i\Delta\tau}\ , \\
f_2^{\pm}(E) &= \frac{1}{E-E_2\pm\frac{i}{2}\Gamma_{10}\pm i\Delta\sigma}\ , \\
f_0 &= 1-\frac{\Delta\rho_0}{\Gamma_{10}-\Delta\rho}\ . \qquad (40)
\end{aligned}
$$

Eq. (39) constitutes the main result of the theoretical part of this paper. Under perfectly controlled approximations, we have derived an expression for the intensity which embodies the Brink–Axel hypothesis and which describes the formation of the DGDR as a transport process.

4.2 Intraband Intensity

We now calculate the intensity $\overline{I_2^{\rm intra}(E)}$ which would result if only the ground state and the one–phonon state could absorb dipole radiation. In other words, we suppress dipole absorption by the states labelled $|0k\rangle$, although we do keep the dynamical coupling of all the states as described by the matrix $H_{\rm eff}$ defined in Eq. (4). We do so in order to distinguish the dipole excitation taken into account by the usual approach to the problem, from the transport process described by Eq. (39). This intensity is defined as

$$\begin{aligned} I_2^{\rm intra}(E) = -\frac{2}{\pi\hbar^4}\int_{-\infty}^{+\infty} dt_1 \int_{-\infty}^{0} d\tau_2 \int_{-\infty}^{+\infty} dt_1' \int_{-\infty}^{0} d\tau_2'\; h(t_1)h(t_1+\tau_2)h^*(t_1')h^*(t_1'+\tau_2') \\ \times \exp[i(E-E_0)(t_1-t_1')/\hbar] \int_{-\infty}^{\infty} d\epsilon \int_{-\infty}^{\infty} d\epsilon' \exp\{i(\epsilon-E_0)\tau_2/\hbar\} \\ \times \exp\{-i(\epsilon'-E_0)\tau_2'/\hbar\}\langle 00|D|10\rangle\langle 10|\frac{1}{\epsilon'-H_{22}-\Sigma_1}|10\rangle\langle 10|D|20\rangle \\ \times\langle 20|{\rm Im}(\frac{1}{E-E_2+E_1-H_{22}+\Sigma_2})|20\rangle \\ \times\langle 20|D|10\rangle\langle 10|\frac{1}{\epsilon-H_{22}+\Sigma_1}|10\rangle\langle 10|D|00\rangle\ . \end{aligned} \tag{41}$$

The ensemble average is given by

$$\begin{aligned} \overline{I_2^{\rm intra}(E)} = 2\pi\times 2\times(\frac{D}{\hbar})^4 \int_{-\infty}^{+\infty} dt_1 \int_{-\infty}^{0} d\tau_2 \int_{-\infty}^{+\infty} dt_1' \int_{-\infty}^{0} d\tau_2'\; h(t_1)h(t_1+\tau_2)h^*(t_1')h^*(t_1'+\tau_2') \\ \times \exp[i(E-E_0)(t_1-t_1')/\hbar]\frac{\Gamma_{20}}{(E-E_2)^2+\frac{1}{4}\Gamma_{20}^2}\exp\{i(E_1-E_0-i/2\Gamma_{10})\tau_2/\hbar\} \\ \times \exp\{-i(E_1-E_0+i/2\Gamma_{10})\tau_2'/\hbar\}\ . \end{aligned} \tag{42}$$

The factor 2 arises because the dipole transition $|10\rangle \to |20\rangle$ is twice as strong as the transition $|00\rangle \to |10\rangle$. We note that when Γ_{10} and Γ_{20} go to zero, $\overline{I_2^{\rm intra}(E)}$ is identical to the harmonic limit denoted by $I_2^{\rm har}(E)$.

For the discussion of our results and the comparison with experimental data, it is useful to also give the average intensity $\overline{I_1(E)}$ for the excitation of the GDR. It is calculated similarly and given by

$$\overline{I_1(E)} = \frac{D^2}{2\pi\hbar^2}\int_{-\infty}^{+\infty} dt_1 \int_{-\infty}^{+\infty} dt_1'\; h(t_1)h^*(t_1')\exp[i(E-E_0)(t_1-t_1')/\hbar]\frac{\Gamma_{10}}{(E-E_1)^2+\frac{1}{4}\Gamma_{10}^2}\ . \tag{43}$$

4.3 Cross Sections

The cross section for the DGDR excitation is given by

$$\sigma_2(E) = 2\pi\int_{b_{\rm min}}^{\infty} b\; db\; \overline{I_2(E)}\ . \tag{44}$$

Here $b_{\min}$ is the minimal impact parameter which is introduced in order to account for the strong absorption that occurs as soon as the colliding nuclei come within reach of their nuclear forces. The cross section $\sigma_1(E)$ for single dipole excitation is defined analogously. We also define

$$\sigma_2(E)^{\rm intra} = 2\pi \int_{b_{\min}}^{\infty} b\, db\, \overline{I_2^{\rm intra}(E)} \tag{45}$$

and

$$\sigma_2^{\rm har}(E) = 2\pi \int_{b_{\min}}^{\infty} b\, db\, I_2^{\rm har}(E)\ . \tag{46}$$

We define two enhancement factors. The first one compares our result with the harmonic limit and is defined as

$$R_1 = \frac{\int_{-\infty}^{\infty}\ dE\sigma_2(E)}{\int_{-\infty}^{\infty}\ dE\sigma_2^{\rm har}(E)}\ . \tag{47}$$

The second factor compares our result with the cross section calculated without the Brink–Axel hypothesis and is defined as

$$R_2 = \frac{\int_{-\infty}^{\infty}\ dE\sigma_2(E)}{\int_{-\infty}^{\infty}\ dE\sigma_2^{\rm intra}(E)}\ . \tag{48}$$

It is also of interest to compare $\sigma_2^{\rm intra}(E)$ with the harmonic approximation. This is accomplished by the third factor

$$R_1^{\rm intra} = \frac{\int_{-\infty}^{\infty}\ dE\sigma_2^{\rm intra}(E)}{\int_{-\infty}^{\infty}\ dE\sigma_2^{\rm har}(E)}\ . \tag{49}$$

The contribution of the extraband excitation is measured by the following two ratios,

$$R_1^{\rm extra} = \frac{\int_{-\infty}^{\infty}\ dE(\sigma_2(E) - \sigma_2^{\rm intra}(E))}{\int_{-\infty}^{\infty}\ dE\sigma_2^{\rm har}(E)}\ , \tag{50}$$

$$R_2^{\rm extra} = \frac{\int_{-\infty}^{\infty}\ dE(\sigma_2(E) - \sigma_2^{\rm intra}(E))}{\int_{-\infty}^{\infty}\ dE\sigma_2^{\rm intra}(E)}\ . \tag{51}$$

We note that $R_1^{\rm extra}$ and $R_2^{\rm extra}$ also account for the contribution of interference terms between the intraband and extraband excitations.

5 Numerical Results

For the calculation of the decay widths $\Gamma_{10}^{\uparrow}, \Gamma_1^{\uparrow}, \Gamma_{20}^{\uparrow}$ and $\Gamma_2^{\uparrow}$, we have used the computer code developed by E. Sheldon and V. C. Rogers [20]. It contains a global optical–model potential to compute the transmission coefficients of nucleons. These in turn were used to determine the mean absorption cross section using the exciton model [21]: The average decay rate of a state

with n excitons into a channel where the nucleon has (asymptotic) kinetic energy ϵ_k is given by [21]

$$w_n(\epsilon_k) = \frac{2m\epsilon_k}{\pi^2\hbar^3}\sigma(\epsilon_k)\frac{\rho_{n-1}(p-1,h,U-E_b-\epsilon_k)}{\rho_n(p,h,U)} \ , \tag{52}$$

where m is the reduced mass, U the excitation energy of the residual nucleus, E_b the separation energy of particle b and $\sigma(\epsilon_k)$ the mean absorption cross section. The function $\rho_n(p,h,U)$ is the n–exciton state density with excitation energy U,

$$\rho_n(p,h,U) = \frac{g}{p!h!(p+h-1)!}(Ug)^{p+h-1} \ . \tag{53}$$

Here g is single–particle level density, p and h are the numbers of particles and holes, and $n = p + h$. The decay width is given by

$$\Gamma^{\uparrow} = \hbar \sum_b \int_0^{E-E_b} w_n(\epsilon_k)\mathrm{d}\epsilon_k \ . \tag{54}$$

The decay widths $\Gamma^{\uparrow}_{10}$ and $\Gamma^{\uparrow}_{1}$ are evaluated at energy E_1, and $\Gamma^{\uparrow}_{20}$ and $\Gamma^{\uparrow}_{2}$ at energy E_2.

In the long–wavelength approximation [22] where the impact parameter b is large compared to the nuclear radius r, the time–dependent function $h(t)$ is given by

$$h(t) = \frac{\gamma}{b^2}\frac{1+\gamma\tau}{(1+\tau^2)^{3/2}} - i\ \frac{\gamma v\omega}{b}\frac{1}{(1+\tau^2)^{1/2}} \ . \tag{55}$$

Here $\tau = \gamma\ v\ t/b$ with $\gamma = 1/\sqrt{(1-v^2/c^2)}$, v is the relative velocity, and $\omega = (E_f - E_i)/\hbar$. The validity of the long–wavelength approximation was checked [23] for giant resonance excitation in the process ^{208}Pb + ^{208}Pb at 640 MeV/A and was found to be accurate to within a few percent.

We consider the DGDR excitation of a ^{208}Pb projectile, incident on a ^{208}Pb target. This reaction has been studied at 640 MeV/A at the GSI/SIS, Darmstadt [7]. We apply the formalism developed in the preceding Sections to calculate the cross section, enhancement factors, and the DGDR width. Using the method described above and with $p = h$ the values $p = 1$ for $\Gamma^{\uparrow}_{10}$, $p = 2$ for $\Gamma^{\uparrow}_{1}$, $p = 2$ for $\Gamma^{\uparrow}_{20}$, and $p = 3$ for $\Gamma^{\uparrow}_{2}$, we find for the decay widths the values $\Gamma^{\uparrow}_{10} = 0.11$ MeV, $\Gamma^{\uparrow}_{20} = 0.026$ MeV, $\Gamma^{\uparrow}_{1} = 0.30$ MeV and $\Gamma^{\uparrow}_{2} = 0.16$ MeV. We set $E_1 - E_0$ and $E_2 - E_0$ equal to their experimental values 13.5 MeV and 27.0 MeV, respectively. The parameter ω appearing in the parametrization (55) of $h(t)$ was accordingly chosen as $\hbar\omega = 13.5$ MeV. Various parametrizations of b_{min} with regard to the nuclear system have been proposed. Most widely used are those of Ref. [24],

$$b_{min} = 1.34(A_1^{1/3} + A_2^{1/3} - 0.75(A_1^{-1/3} + A_2^{-1/3})) \text{ (fm)} \tag{56}$$

and of Ref. [25],

$$b_{min} = 1.1(A_1^{1/3} + A_2^{1/3} + \frac{A_1^{1/3} A_2^{1/3}}{A_1^{1/3} + A_2^{1/3}} - 1.9) \text{ (fm)} . \tag{57}$$

For the system ^{208}Pb + ^{208}Pb, Eqs. (56) and (57) yield $b_{min} = 15.7$ fm and $b_{min} = 14.4$ fm, respectively. We have used the mean of these estimated values, $b_{min} = 15.05$ fm.

In order to calculate the absolute values of the cross sections we evalute the dipole matrix elements by means of the sum rule for dipole transition

$$\sum_f \omega_{fi} |D_{fi}^{(m)}|^2 = \frac{3e^2}{8\pi m_N} \frac{NZ}{A} = S_D . \tag{58}$$

Here $D_{fi}^{(m)} = \int r Y_{1m}(\hat{r}) \rho(r) dv$. In practice, we use

$$\sum_f \omega_{fi} |D^2| = \frac{4\pi}{3} S_D, \tag{59}$$

with $D = \int x\rho(r)dv = \int z\rho(r)dv$. Unless otherwise stated, we always use 100% of the sum rule.

Particular attention must be paid to the spreading widths as these determine largely the outcome of the calculation. Here, we repeat a statement already made in the Introduction: This paper is primarily devoted to the implementation of the Brink–Axel hypothesis, to the derivation of an expression for the average cross section based on this hypothesis and on controlled approximations, and to the investigation of the consequences of this hypothesis for the excitation cross section of the DGDR. In this sense, we consider the various spreading widths as parameters. We are not primarily concerned with assigning physically realistic values to the $\Gamma^{\downarrow}$'s. Still, it is worthwhile to comment on some problems that arise if one tries to do so.

The parameters are the spreading width $\Gamma_2^{\downarrow}$ of the states $|1k\rangle$, the spreading width $\Gamma_{10}^{\downarrow}$ of the one–phonon state $|10\rangle$ (by assumption this width also describes the mixing of the two–phonon state $|20\rangle$ with the states $|1k\rangle$), and the spreading width $\Gamma_{20}^{\downarrow}$ which describes the mixing of the two–phonon state $|20\rangle$ with the states $|0\alpha\rangle$. The total spreading width of the two–phonon state is accordingly given by $\Gamma_{\text{total }20}^{\downarrow} = \Gamma_{10}^{\downarrow} + \Gamma_{20}^{\downarrow}$. We know experimentally the spreading width $\Gamma_{10} = 4.0$ MeV [7] of the one–phonon state. Theoretically Γ_{10} is given by $\Gamma_{10} = \Gamma_{10}^{\uparrow} + \Gamma_{10}^{\downarrow}$. Typically, three effects contribute to the observed spreading width of the GDR: The coupling to the complex modes of excitation contained in our Hamiltonian of Eq. (1), the spread in energy of the single–particle modes which contribute to the GDR (Landau damping), and the coupling to low–lying vibrational modes [26]. This makes it difficult to estimate the spreading width $\Gamma_{\text{total }20}^{\downarrow}$ of the two–phonon state. Neglecting the contribution of Landau damping and of the vibrational

modes to $\Gamma^{\downarrow}_{10}$ altogether and using the exciton model in the form of Ref. [27] (we identify the n–phonon state as a n–particle n–hole configuration), we find that the spreading width $\Gamma^{\downarrow}_{\text{total } n0}$ of the n–phonon states is proportional to $2n$ Im $[V_{\text{opt}}(E_n/2n)]$. Here $V_{\text{opt}}(E)$ is the depth of the optical–model potential at energy E, and E_n is the excitation energy. This relation derives from the fact that each exciton (particle or hole) carries the average energy $(E_n/2n)$. We observe that for $n = 1$ and $n = 2$, the energy arguments of $V_{\text{opt}}(E_n/2n)$ coincide, yielding $\Gamma^{\downarrow}_{\text{total } 20} = 2\Gamma^{\downarrow}_{10}$. This result is in keeping with the predictions of the harmonic picture for the n–phonon states and gives $\Gamma^{\downarrow}_{20} = \Gamma^{\downarrow}_{10} = 4.0$ MeV. Comparison with experimental data will show that this is an overestimate which we ascribe to the fact that Landau damping and coupling to the vibrational modes contribute differently to $\Gamma^{\downarrow}_{10}$ and to $\Gamma^{\downarrow}_{20}$. It turns out that $\Gamma^{\downarrow}_{20} \sim 0.5\ \Gamma^{\downarrow}_{10}$ yields results which are in good agreement with the data. Similarly, using the measured value for $\Gamma^{\downarrow}_{10}$ and the exciton model to estimate $\Gamma^{\downarrow}_{2}$ yields an unreasonably large value. We often use $\Gamma^{\downarrow}_{2} = 0.5$ MeV and remark only that our results are insensitive to this choice, see Fig. 5.

Prior to our giving detailed results for the reaction ^{208}Pb on ^{208}Pb at 640 MeV/A (the case studied experimentally), we discuss the dependence of our results on some of the relevant parameters. The following calculations were all done for the reaction ^{208}Pb on ^{208}Pb as described above except that the energy, the decay widths and the spreading widths were varied.

We investigate the dependence of the cross sections for the GDR and DGDR excitation on the spreading width $\Gamma^{\downarrow}_{10}$ and on the projectile energy E_p/A. It is instructive to begin with the GDR excitation. Fig. 2 shows the energy–integrated cross section σ_1 for the GDR excitation as a function of the spreading with $\Gamma^{\downarrow}_{10}$ at various projectile energies. The dependence of σ_1 on $\Gamma^{\downarrow}_{10}$ changes significantly with projectile energy. For the lower projectile energies, the cross section first increases strongly then more slowly and finally decreases as $\Gamma^{\downarrow}_{10}$ increases. For large E_p/A (10000 MeV) the cross section decreases monotonically with increasing $\Gamma^{\downarrow}_{10}$. This dependence can be understood qualitatively with the help of the Weizsaecker-Williams (WW) method of equivalent photons [7, 28]. In this method the transition probability for the GDR excitation at impact parameter b is given by

$$P_{\text{GDR}}(b) = \int N(b, E_\gamma)\sigma_{\text{phot}}(E_\gamma)\frac{dE_\gamma}{E_\gamma}\ . \tag{60}$$

Here $N(b, E_\gamma)$ denotes the number of equivalent photons of frequency $E_\gamma/\hbar$ at impact parameter b, a function of projectile energy, while $\sigma_{\text{phot}}(E_\gamma)$ is the photoabsorption cross section which is well described by a Lorentzian. For small values of the spreading width $\Gamma^{\downarrow}_{10}$, only the photons with frequency close to the central frequency $(E_1 - E_0)/\hbar$ substantially contribute to the

transition probability. As $\Gamma^{\downarrow}_{10}$ increases, an ever wider band of photons contributes to and enhances $P_{\rm GDR}(b)$. On the other hand, the widening of the normalized Lorentzian causes the absorption strength of the photons with frequencies around the central frequency to decrease, which suppresses $P_{\rm GDR}(b)$. These effects compete against each other. The result depends on the distribution of available photons over the relevant frequency range. For small values of E_p/A, $N(b, E_\gamma)$ decreases rapidly with increasing E_γ [29]. In this case the gain of $P_{\rm GDR}(b)$ exceeds the loss unless $\Gamma^{\downarrow}_{10}$ becomes large. As a result, the GDR cross section (an integral of $P_{\rm GDR}(b)$ over impact parameter) increases with $\Gamma^{\downarrow}_{10}$ up to a certain value of the spreading width beyond which the loss surpasses the gain. At very high projectile energy the curve of $N(b, E_\gamma)$ versus E_γ becomes flat [29]. The loss always exceeds the gain, and the cross section decreases monotonically with $\Gamma^{\downarrow}_{10}$. Since $N(b, E_\gamma)$ increases with E_p/A, so do both $P_{\rm GDR}(b)$ and cross section. Fig. 2 shows that the enhancement of the cross section due to the spreading width is most pronounced when E_p/A is around several hundred MeV. We refer to this enhancement as to the damping enhancement. Taking for projectile energy and spreading width the experimental values E_p/A = 640 MeV and $\Gamma^{\downarrow}_{10}$ = 4.0 MeV, we find for the ratio of the energy–integrated cross section with damping to that without damping the value 1.20.

Fig. 3 shows for several projectile energies the dependence of the energy–integrated cross section for the DGDR excitation on the spreading width $\Gamma^{\downarrow}_{10}$. We use the five ratios defined in Section 4.3 to measure the cross sections. We keep the decay widths and the ratio $\Gamma^{\downarrow}_{10}/\Gamma^{\downarrow}_{20}$ fixed. We focus first on the intraband cross section measured by $R_1^{\rm intra}$. The dependence of the intraband cross section on spreading width and projectile energy is similar to that of σ_1 (Fig. 2): At small projectile energies, $R_1^{\rm intra}$ first increases then decreases with increasing $\Gamma^{\downarrow}_{10}$, while it decreases monotonically with $\Gamma^{\downarrow}_{10}$ at high energies. This is because the intraband excitation is governed by two transition probabilities: one for the transition $|00\rangle \rightarrow |10\rangle$, the other for the transition $|10\rangle \rightarrow |20\rangle$. Each of the two probabilities can be described by Eq. (60). Thus, the intraband cross section depends on spreading width and projectile energy in a similar way as σ_1. Some of the probability flux feeding the one–phonon state $|10\rangle$ flows into the states $|0k\rangle$, and – in the intraband approximation – is not available for the second dipole excitation. This flow increases with $\Gamma^{\downarrow}_{10}$. Therefore, the enhancement of $R_1^{\rm intra}$ only survives for rather low projectile energies, and the range in which $R^{\rm intra}$ increases with the spreading width is significantly reduced compared to that of σ_1. The extraband excitation measured by $R_1^{\rm extra}$ (compared with the harmonic limit) and $R_2^{\rm extra}$ (compared with the intraband cross section) increases monotonically

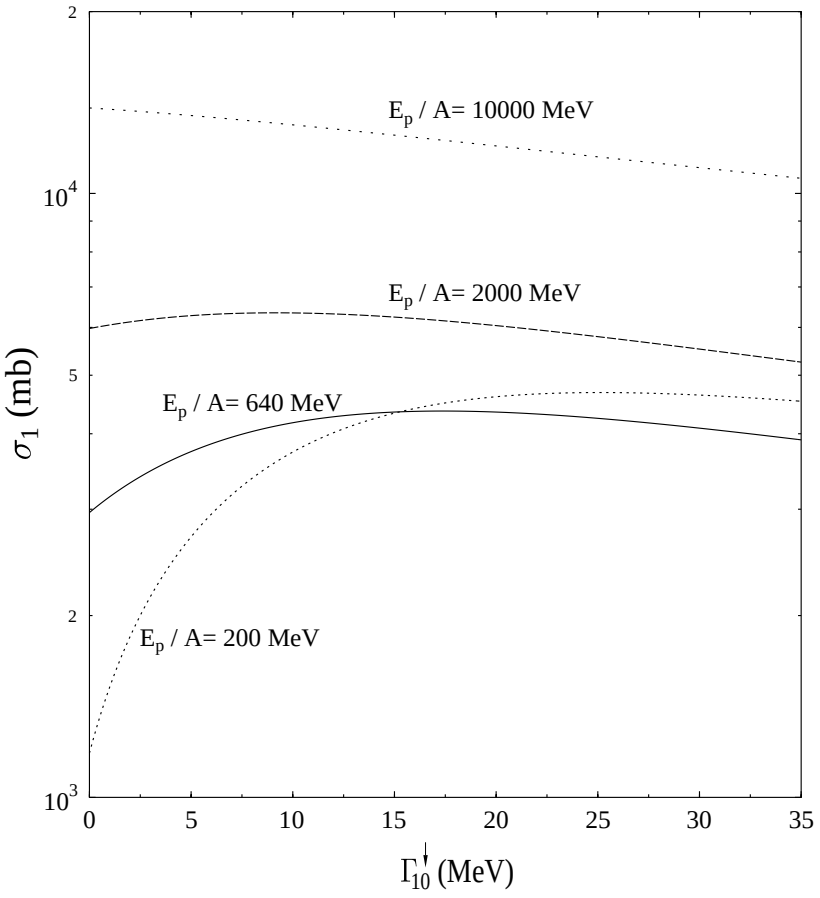

Figure 2: Energy–integrated cross section for the GDR excitation as a function of spreading width $\Gamma_{10}^{\downarrow}$ at different projectile energies E_p/A, with $\Gamma_{10}^{\uparrow} = 0.11$ MeV.

with $\Gamma_{10}^{\downarrow}$. For small projectile energy (E_p/A = 200 MeV) and small values of $\Gamma_{10}^{\downarrow}$ both ratios have small negative values. However, in most cases the extraband excitation gives a positive contribution to the total cross section.

The total cross section is measured by R_1 (compared with the harmonic limit) and by R_2 (compared with the intraband cross section). The ratio R_2 increases monotonically with $\Gamma_{10}^{\downarrow}$ and is larger than unity except for small projectile energy and small $\Gamma_{10}^{\downarrow}$. At the smaller projectile energies, R_1 first increases and later decreases with $\Gamma_{10}^{\downarrow}$. The turning point shifts towards larger values of $\Gamma_{10}^{\downarrow}$ as E_p/A decreases. With increasing E_p/A the range where R_1 is larger than unity disappears. An enhancement of the total cross section compared with the harmonic limit can, therefore, be expected only for low projectile energy. Moreover, this enhancement is not mainly due to the extraband excitation ($R_1^{\rm extra}$ and $R_2^{\rm extra}$ being small), but is mainly due to the damping enhancement discussed for σ_1 above. For the case of E_p/A = 200 MeV and $\Gamma_{10}^{\downarrow}$ = 4.0 MeV, R_1 reaches the value 1.50. For E_p/A = 640 MeV where the measurement was performed and $\Gamma_{10}^{\downarrow}$ = 4.0 MeV, we find R_1 = 1.01: The gain of the total cross section due to extraband transitions just compensates the loss due to the reduction of the intraband cross section, resulting in a zero net enhancement for the total cross section compared with the harmonic limit.

Fig. 4 shows the dependence of the cross sections and enhancement factors for the DGDR excitation on projectile energy. In Fig. 4(a), σ_2, $\sigma_2^{\rm intra}$, $\sigma_2^{\rm har}$ and $\sigma_2^{\rm extra}$ are the total, intraband, harmonic limit and extraband energy–integrated cross sections, respectively. (Actually, $\sigma_2^{\rm extra}$ is not a cross section itself but rather the difference of two cross sections). All of the cross sections increase monotonically with E_p/A. The total cross section largely stems from intraband excitation. The extraband transition contributes not more than 10% compared with the harmonic limit. For $E_p/A < 420$ MeV, $\sigma_2^{\rm intra}$ is larger than $\sigma_2^{\rm har}$. This indicates once again the damping enhancement which occurs at lower projectile energies where the extraband contribution is negligible. For very low projectile energy, the enhancement factors R_1 and $R_1^{\rm intra}$ can reach several hundred percent. This results from the damping enhancement. When E_p/A is larger than 500 MeV, R_2, $R_2^{\rm extra}$ and $R_1^{\rm extra}$ are constant with values below 1.10 and 0.1, respectively.

We turn to the dependence of the cross section for the DGDR excitation on the parameters $\Gamma_{10}^{\uparrow}$, $\Gamma_{20}^{\uparrow}$, $\Gamma_{1}^{\uparrow}$, $\Gamma_{2}^{\uparrow}$, $\Gamma_{20}^{\downarrow}$ and $\Gamma_{2}^{\downarrow}$, using R_1 and $R_1^{\rm intra}$. We note that the parameters $\Gamma_{2}^{\uparrow}$, $\Gamma_{2}^{\downarrow}$, $\Gamma_{20}^{\uparrow}$ and $\Gamma_{20}^{\downarrow}$ appear in the expression for the cross section only in the combinations $\Gamma_{2}^{\uparrow}+\Gamma_{2}^{\downarrow}$ and $\Gamma_{20}^{\uparrow}+\Gamma_{20}^{\downarrow}$.

Fig. 5(a) shows R_1 and $R_1^{\rm intra}$ as functions of $\Gamma_{10}^{\uparrow}$. The ratios decrease with increasing $\Gamma_{10}^{\uparrow}$, and are reduced by almost a factor of two when $\Gamma_{10}^{\uparrow}$ is as large as several MeV. For realistic

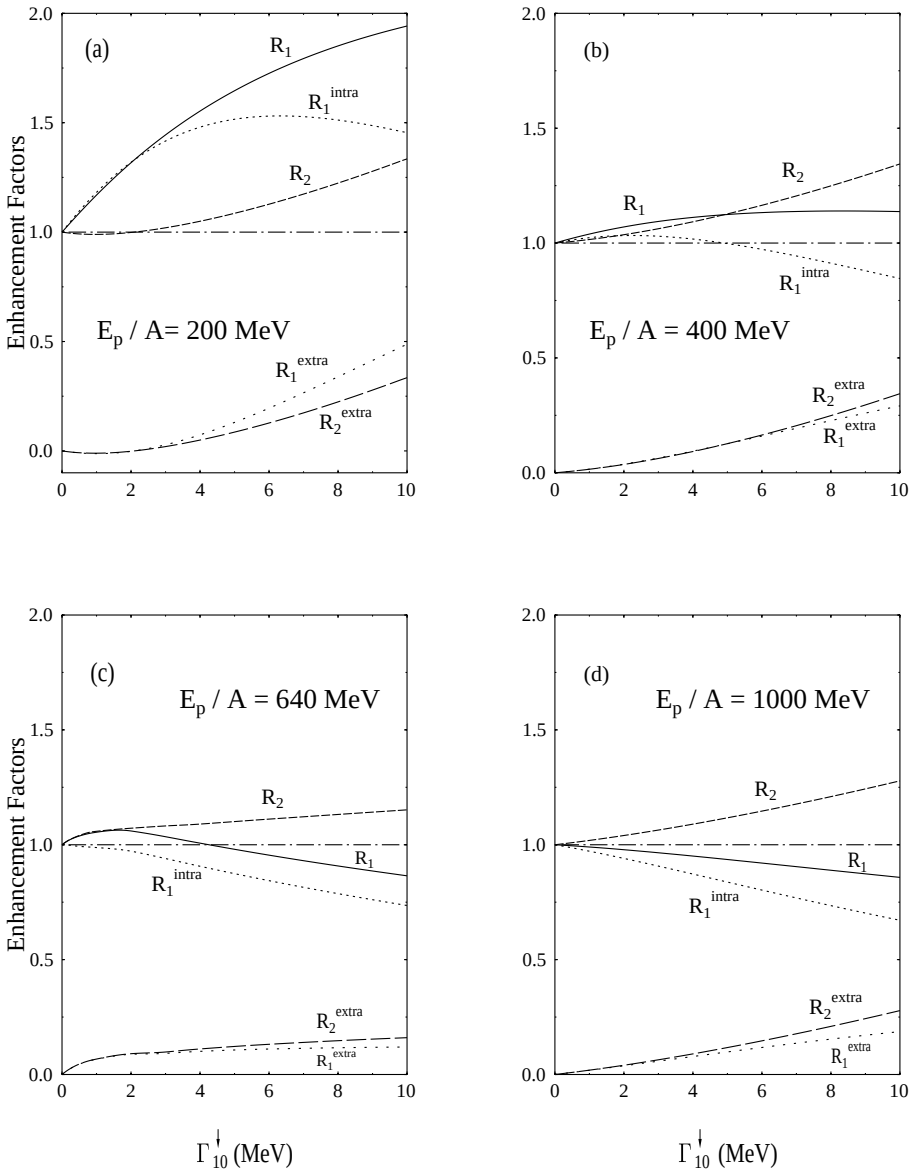

Figure 3: Enhancement factors for the energy–integrated cross sections for DGDR excitation as described in the text as functions of $\Gamma_{10}^{\downarrow}$ at different projectile energies. Parameter values are $\Gamma_{10}^{\uparrow} = 0.11$, $\Gamma_{20}^{\uparrow} = 0.026$, $\Gamma_{1}^{\uparrow} = 0.30$, $\Gamma_{2}^{\uparrow} = 0.16$, $\Gamma_{20}^{\downarrow} = 0.5\Gamma_{10}^{\downarrow}$ and $\Gamma_{2}^{\downarrow} = 0.5$ (MeV).

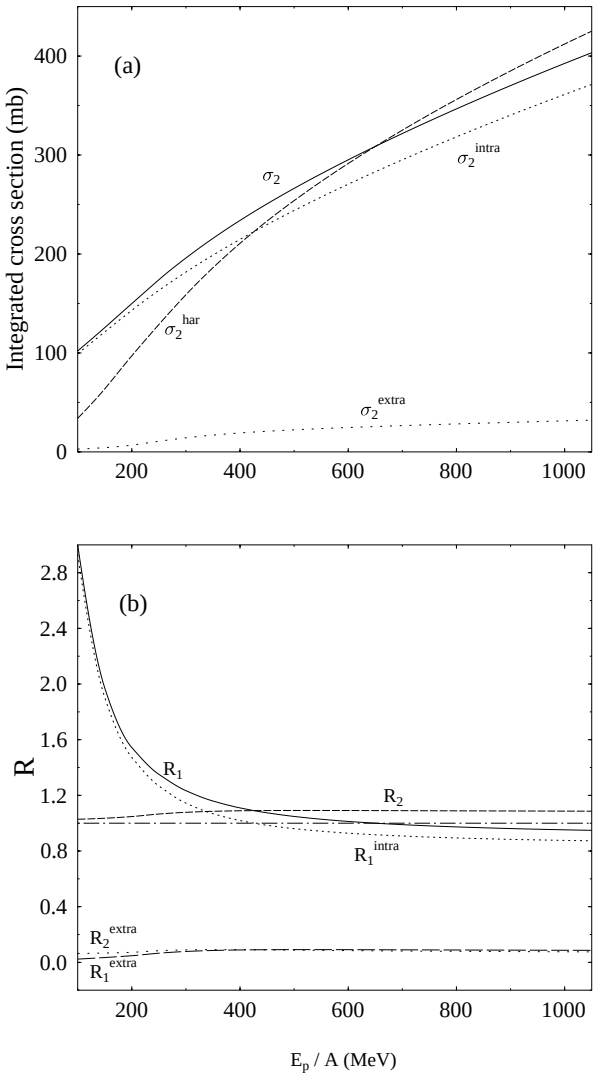

Figure 4: (a) Energy–integrated cross sections and (b) enhancement factors for the DGDR excitation versus E_p/A. Parameter values are $\Gamma^{\uparrow}_{10} = 0.11$, $\Gamma^{\uparrow}_{20} = 0.026$, $\Gamma^{\downarrow}_{10} = 4.0$, $\Gamma^{\uparrow}_{1} = 0.30$, $\Gamma^{\uparrow}_{2} = 0.16$, $\Gamma^{\downarrow}_{20} = 0.5\Gamma^{\downarrow}_{10}$ and $\Gamma^{\downarrow}_{2} = 0.5$ (MeV).

values of $\Gamma_{10}^{\uparrow}$ the reduction is quite small, however. An increase of $\Gamma_{10}^{\uparrow}$ reduces the lifetime of the one–phonon state and suppresses the intraband excitation which dominates the DGDR excitation (Fig. 4). Both ratios depend only weakly or not at all on $\Gamma_1^{\uparrow}$ (Fig. 5(b)). It is clear that the dominant intraband excitation is independent of $\Gamma_1^{\uparrow}$. The slow decrease of R_1 with increasing $\Gamma_1^{\uparrow}$ is due to the loss of extraband transition strength. However, the latter gives only a small contribution to R_1. In Fig. 5(c) and Fig. 5(d) we display the dependence of R_1 and of $R_1^{\rm intra}$ on $\Gamma_2^{\uparrow} + \Gamma_2^{\downarrow}$ and on $\Gamma_{20}^{\uparrow} + \Gamma_{20}^{\downarrow}$, respectively. In both cases R_1 increases with the increase of the variable. However, this increase is so slow that the precise choice of these parameters is irrelevant for our calculations. The two variable combinations on the abscissas of Figs. 5(c) and 5(d) do not cause any loss of probability flux feeding the DGDR. Therefore, we attribute the slow rise of R_1 in both figures to damping enhancement. This is obvious for Fig. 5(c) where the intraband cross section is independent of $\Gamma_2^{\uparrow} + \Gamma_2^{\downarrow}$ and where the increase of R_1 is due to the damping enhancement for the transition $|0k\rangle \rightarrow |1k\rangle$. In Fig. 5(d) damping enhancement works also for $R_1^{\rm intra}$. It is interesting to see that the damping enhancement survives (albeit weakly) even if E_p/A is as high as 640 MeV.

We turn to a comparison of our results with experimental data [30]. In keeping with experimental results [31], we use 122% of the sum rule for all dipole matrix elements. Fig. 6 shows the differential cross section for the DGDR excitation as a function of excitation energy. The cross section has been normalized to its maximum value. The width of the DGDR is 6.1 MeV. Integrating the differential cross section over excitation energy from neutron threshold at 7.5 MeV up to 40.0 MeV (this corresponds to the experimental situation), we find the value 410 mb. This value is somewhat larger than that given in Ref. [30], 380 $\pm$ 40 mb, where the folding method [32] is used. Both our DGDR width and energy–integrated cross section are consistent, however, with the experimental values within experimental errors. In the present case, the enhancement factor R_1 is 1.03, almost the same as shown in Fig. 3. In Fig. 7, we plot the ratio of the energy–integrated cross sections for the DGDR and the GDR as a function of $\Gamma_{10}^{\downarrow}$. The ratio first increases and then decreases as this parameter increases. At the experimental value $\Gamma_{10}^{\downarrow} = 4.0$ MeV, the ratio is 0.0988, which again agrees with experiment (0.11 $\pm$ 0.013 [30]) within the experimental error.

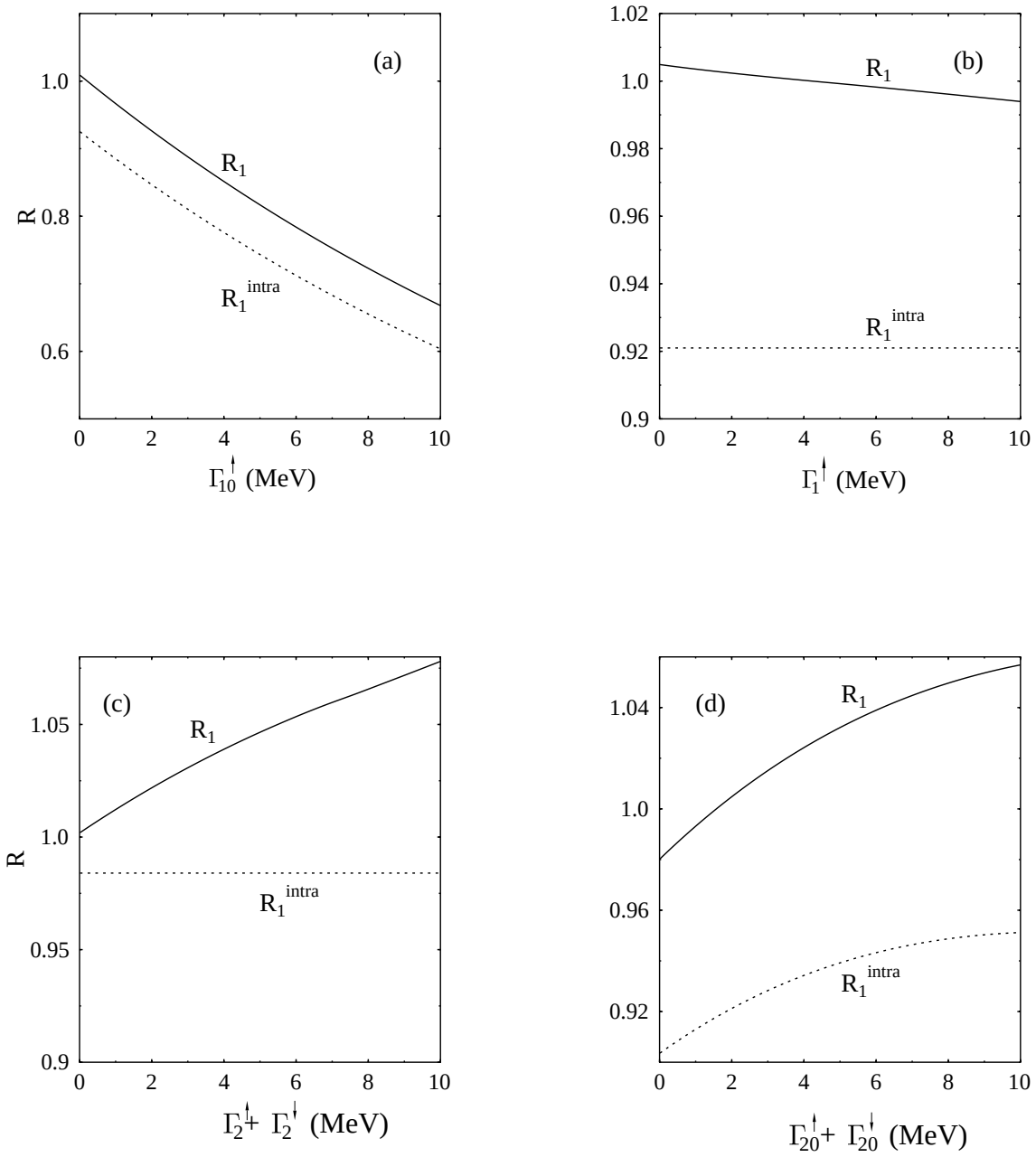

Figure 5: Enhancement factors of the energy–integrated cross sections for DGDR excitation versus (a) $\Gamma^{\uparrow}_{10}$, (b) $\Gamma^{\uparrow}_{1}$, (c) $\Gamma^{\uparrow}_{2} + \Gamma^{\downarrow}_{2}$ and (d) $\Gamma^{\uparrow}_{20} + \Gamma^{\downarrow}_{20}$. Parameter values are $E_p/A = 640$, $\Gamma^{\downarrow}_{10} = 4.0$, $\Gamma^{\downarrow}_{20} = 0.5\Gamma^{\downarrow}_{10}$, (a) $\Gamma^{\uparrow}_{20} = 0.026$, $\Gamma^{\uparrow}_{1} = 0.30$, $\Gamma^{\uparrow}_{2} = 0.16$, $\Gamma^{\downarrow}_{2} = 0.5$; (b) $\Gamma^{\uparrow}_{10} = 0.11$, $\Gamma^{\uparrow}_{20} = 0.026$, $\Gamma^{\uparrow}_{2} = 0.16$, $\Gamma^{\downarrow}_{2} = 0.5$; (c) $\Gamma^{\uparrow}_{10} = 0.11$, $\Gamma^{\uparrow}_{20} = 0.026$, $\Gamma^{\uparrow}_{1} = 0.30$; (d) $\Gamma^{\uparrow}_{10} = 0.11$, $\Gamma^{\uparrow}_{1} = 0.30$, $\Gamma^{\uparrow}_{2} = 0.16$, $\Gamma^{\downarrow}_{2} = 0.5$ (MeV).

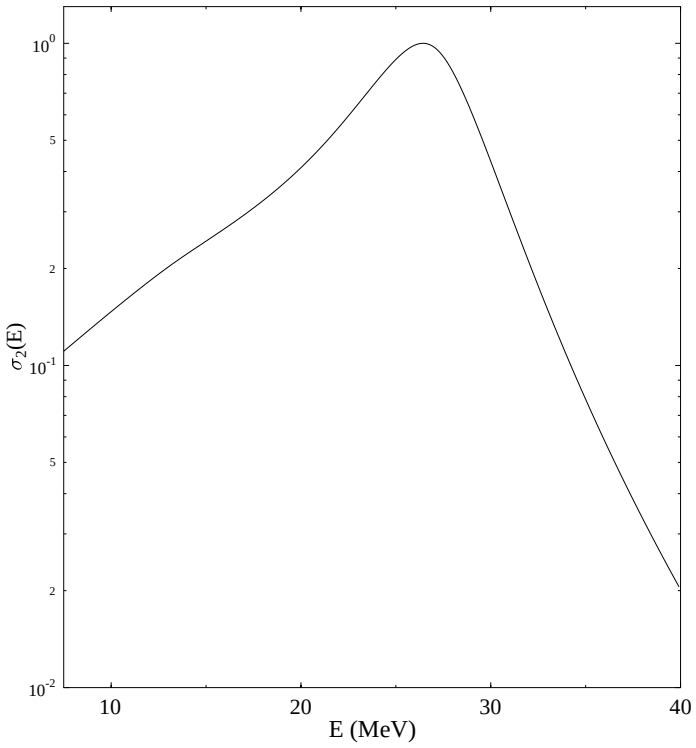

Figure 6: Differential cross section for the DGDR excitation versus excitation energy. Parameter values are $b_{min} = 15.5$ fm, $E_p/A = 640$, $\Gamma^{\uparrow}_{10} = 0.11$, $\Gamma^{\uparrow}_{20} = 0.026$, $\Gamma^{\uparrow}_{1} = 0.30$, $\Gamma^{\uparrow}_{2} = 0.16$, $\Gamma^{\downarrow}_{10} = 4.0$, $\Gamma^{\downarrow}_{20} = 0.5\Gamma^{\downarrow}_{10}$ and $\Gamma^{\downarrow}_{2} = 0.5$ (MeV).

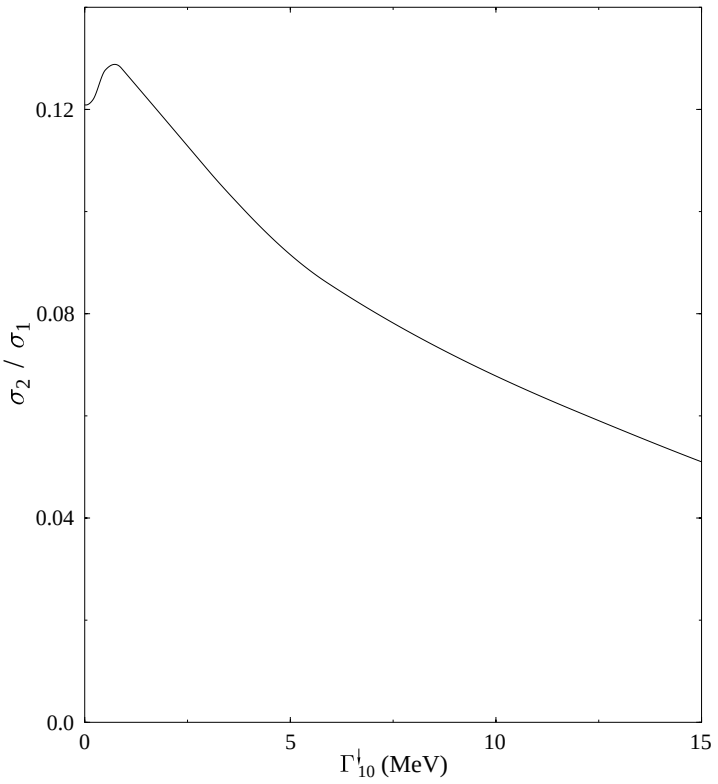

Figure 7: Ratio of energy–integrated cross sections for the DGDR and GDR excitation versus spreading width $\Gamma^{\downarrow}_{10}$. Parameter values are $b_{min} = 15.5$ fm, $E_p/A = 640$, $\Gamma^{\uparrow}_{10} = 0.11$, $\Gamma^{\uparrow}_{20} = 0.026$, $\Gamma^{\uparrow}_{1} = 0.30$, $\Gamma^{\uparrow}_{2} = 0.16$, $\Gamma^{\downarrow}_{20} = 0.5\Gamma^{\downarrow}_{10}$ and $\Gamma^{\downarrow}_{2} = 0.5$ (MeV).

6 Comparison with the approach by Carlson *et al.*

As mentioned in Section 1, Carlson *et al.* [11, 12] implemented the Brink–Axel hypothesis using a statistical model developed by Ko [14]. The model of Ref. [11, 12] differs from the one used here mainly in terminology: The authors use a direct product representation of Hilbert space rather than the direct sum representation of our Eq. (1). In Refs. [11, 12] the states in Hilbert space are written in the form $|n\alpha\rangle$. Here n denotes the number $n = 0, 1, \ldots$ of phonons and α enumerates the background states. As a consequence, the mixing of the one–phonon state with the background states is formally described as a de–excitation of the former, i.e., as the transition $|10\rangle \to |0\alpha\rangle$. The Brink–Axel hypothesis is automatically implemented because dipole excitation affects only the first component n in the state labelled $|n\alpha\rangle$. As far as we can see, the physical content of both models is quite the same, however. The main difference between both approaches lies in the analytical evaluation of the average cross section. Indeed, in Refs. [11, 12] the average over the background components labelled α is performed over the Green function (rather than over the intensity) and, although intuitively reasonable, does not involve controlled approximations. We are, in fact, not able to say whether the statistical assumptions invoked in Refs. [11, 12] are the same as ours or not. In contradistinction to this procedure, we have averaged in Section 4 the intensity, and we have reduced the resulting expression by controlled approximations to the final form of Eq. (39). We are sure that for realistic values of the decay widths, the statistical error of this equation and the cross section formulas derived from it, is less than one percent. The terminology differs also regarding the term "harmonic approximation". In Refs. [11, 12], this term denotes what is here called the intraband transition.

The numerical calculations of Carlson *et al.* [11, 12] are quite different in detail from the ones performed here. This is why we can only compare the results and not the intermediate steps. We do this for the reaction of ^{208}Pb on ^{208}Pb at 640 MeV discussed throughout this paper. For the ratio of the energy–integrated cross section over the energy–integrated intraband cross section (we recall that this is referred to as the harmonic approximation cross section in Refs. [11, 12]), Carlson *et al.* find the value 120%. This has to be compared with our value 108%. We conclude that the approach of Carlson *et al.* [11, 12] constitutes a fair approximation to the exact value.

7 Summary

We have studied the DGDR excitation using the Brink–Axel mechanism. The background states which couple to the one–phonon and two–phonon states are described in terms of the Gaussian Orthogonal Ensemble of random matrices. We use second–order time–dependent perturbation theory and calculate analytically the ensemble–averaged cross section for the DGDR excitation. This quantity is a function of the various decay widths and spreading widths of the one–phonon, two–phonon, and background states. The decay widths have been calculated from the optical model and the exciton model. The spreading widths are taken from experiment or used as parameters. We have numerically studied the dependence of the cross section for excitation of the DGDR on the various parameters of the theory. We have shown that for realistic values of these parameters, the contribution to the cross section from the Brink–Axel mechanism is significant. This is especially true for the reaction ^{208}Pb + ^{208}Pb at projectile energy 640 MeV/nucleon. We have compared our results with those of Carlson *et al.* and have found that their work provides a fair approximation. For sensible values of the various spreading widths, we find that the width of the DGDR, the value of the energy–integrated cross section, and the ratio of this quantity over the energy–integrated cross section for single GDR excitation, all agree with experiment within experimental errors. We take this as a strong indication that the present approach accounts quantitatively for the DGDR excitation. It would not be difficult to use our Eq. (39) for the analysis of other data sets. Clearly, the formalism can be extended to triple–phonon excitation.

Acknowledgment. We are grateful to A. Bulgac, B. Carlson, L. Canto, H. Emling, M. Hussein, C. Lewenkopf, and J. Li for discussions, and to H. Emling for very helpful suggestions.

References

[1] R. Schmidt *et al.*, Phys. Rev. Lett. **70** (1993) 1767.

[2] T. Aumann *et al.*, Phys. Rev. C **47** (1993) 1728.

[3] J. Ritman *et al.*, Phys. Rev. Lett. **70** (1993) 533.

[4] J. R. Beene, Nucl. Phys. A **569** (1993) 163c.

[5] G. Baur and C. A. Bertulani, Phys. Lett. B **174** (1986) 23.

[6] T. Aumann, C. A. Bertulani and K. Sümmerer, Phys. Rev. C **51** (1995) 416.

[7] H. Emling, Prog. Part. Nucl. Phys. **33** (1994) 729.

[8] C. Volpe *et al.*, Nucl. Phys. A **589** (1995) 521.

[9] P. F. Bortignon and C. H. Dasso, Phys. Rev. C **56** (1997) 574.

[10] M. S. Hussein, A. F. R. de Toledo Piza and O. K. Vorov, Phys. Rev. C **59** (1999) R1242.

[11] B. V. Carlson *et al.*, Ann. Phys. (N. Y.) **276** (1999) 111.

[12] B. V. Carlson *et al.*, Phys. Rev. C **60** (1999) 014604.

[13] D. Brink, D. Phil. thesis, Oxford University (unpublished), 1955; P. Axel, Phys. Rev. **126** (1962) 671.

[14] C. M. Ko, Z. Phys. A **286** (1978) 405.

[15] M. L. Mehta, Random Matrices, 2nd Ed., Academic Press (New York) 1991.

[16] T. Guhr, A. Müller-Groeling and H. A. Weidenmüller, Phys. Rep. **299** (1998) 189.

[17] K. Alder and A. Winther, Coulomb Excitation, Academic Press (New York) 1965.

[18] J. J. M. Verbaarschot, H. A. Weidenmüller and M. R. Zirnbauer, Phys. Rep. **129** (1985) 367.

[19] J. Z. Gu and H. A. Weidenmüller, Nucl. Phys. A **660** (1999) 197.

[20] E. Sheldon and V. C. Rogers, Computer Phys. Commun. **6** (1973) 99.

[21] G. Mantzouranis, H. A. Weidenmüller and D. Agassi, Z. Phys. A **276** (1976) 145.

[22] C. A. Bertulani and V. Zelevinsky, Nucl. Phys. A **568** (1994) 931.

[23] E. G. Lanza, Nucl. Phys. A **613** (1997) 445.

[24] C. J. Benesh, B. C. Cook and J. P. Vary, Phys. Rev. C **40** (1989) 1198.

[25] S. Kox *et al.*, Phys. Rev. C **35** (1987) 1678.

[26] G. F. Bertsch, P. F. Bortignon and R. A. Broglia, Rev. Mod. Phys. **55** (1983) 287.

[27] M. Herman, G. Reffo and H. A. Weidenmüller, Nucl. Phys. A **536** (1992) 124.

[28] C. A. Bertulani and G. Baur, Phys. Rep. **163** (1988) 299.

[29] W. J. Llope and P. Braun-Munzinger, Phys. Rev. C **41** (1990) 2644.

[30] K. Boretzky *et al.*, Phys. Lett. B **384** (1996) 30.

[31] D. Schelhaas *et al.*, Nucl. Phys. **A 489** (1988) 189.

[32] T. Aumann, P. F. Bortignon, and H. Emling, Ann. Rev. Nucl. Part. Sci. **48** (1998) 351.

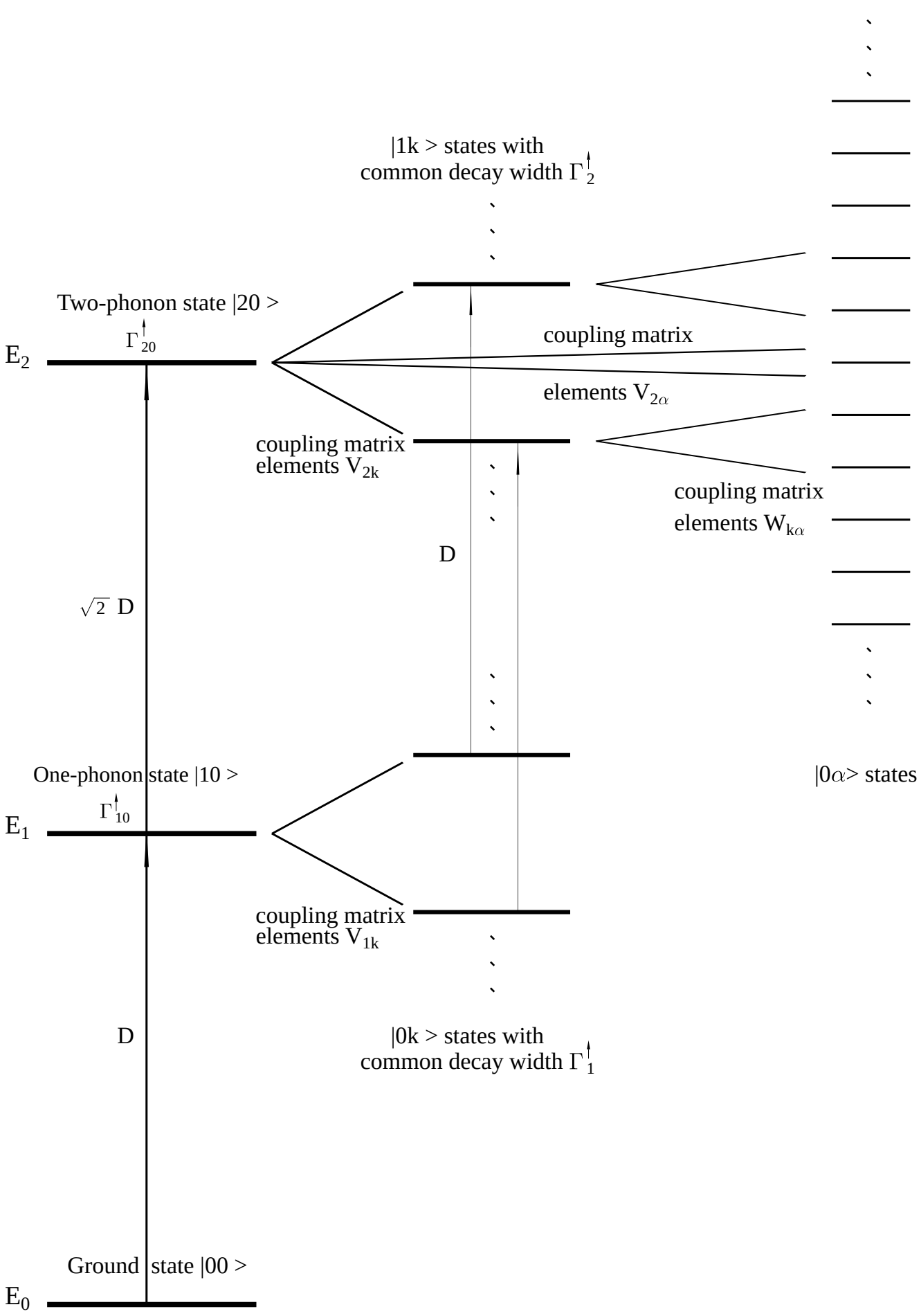
|1k > states with
common decay width Γ2
Two-phonon state |20 >
Γ20
E2
coupling matrix
elements V2α
coupling matrix
elements V2k
coupling matrix
elements Wkα
D
√2 D
One-phonon state |10 >
Γ10
E1
|0α> states
coupling matrix
elements V1k
D
|0k > states with
common decay width Γ1
Ground state |00 >
E0

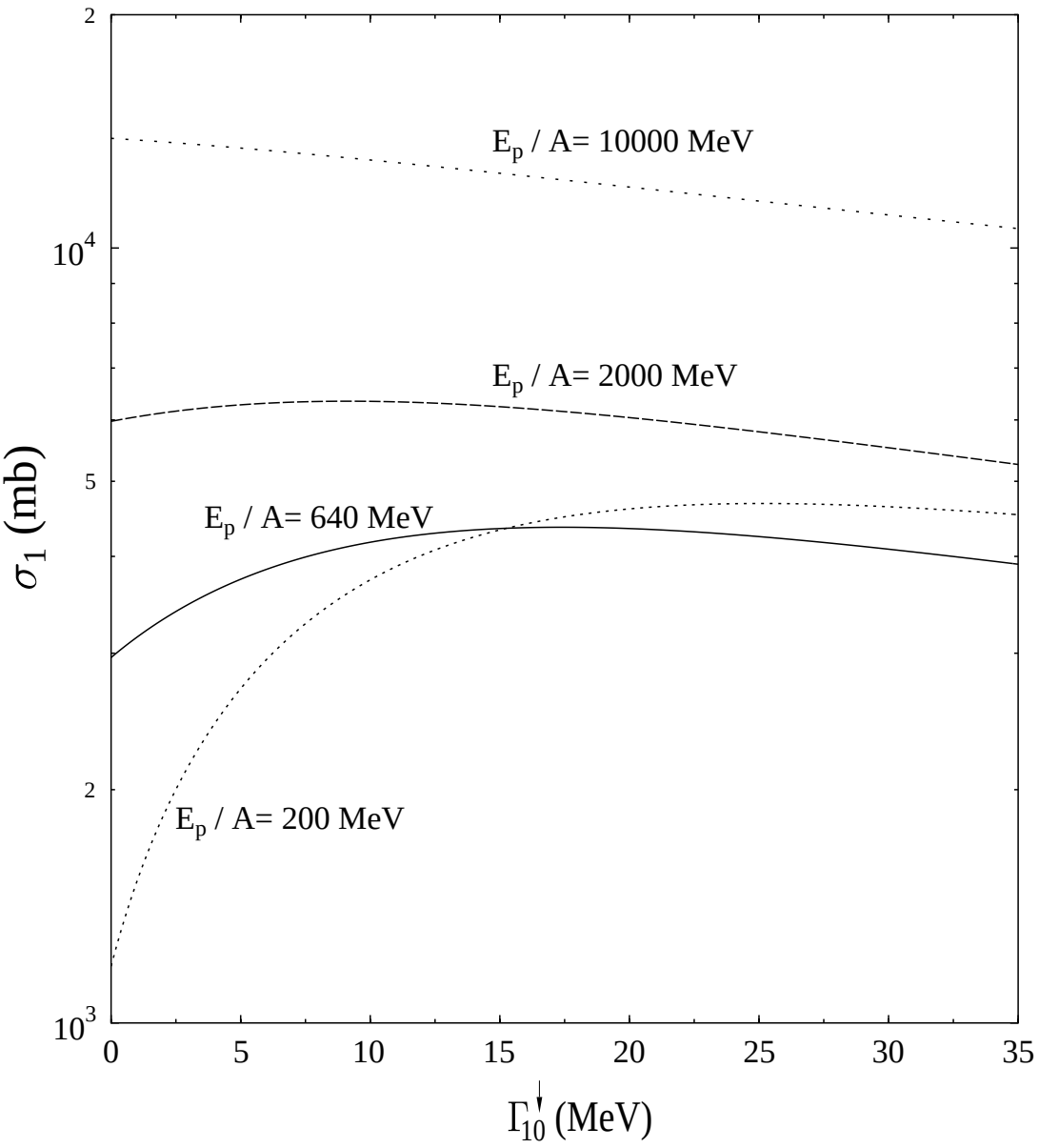
2
10^4
5
2
10^3
σ_1 (mb)
E_p / A= 10000 MeV
E_p / A= 2000 MeV
E_p / A= 640 MeV
E_p / A= 200 MeV
0
5
10
15
20
25
30
35
$\Gamma_{10}^{\downarrow}$ (MeV)

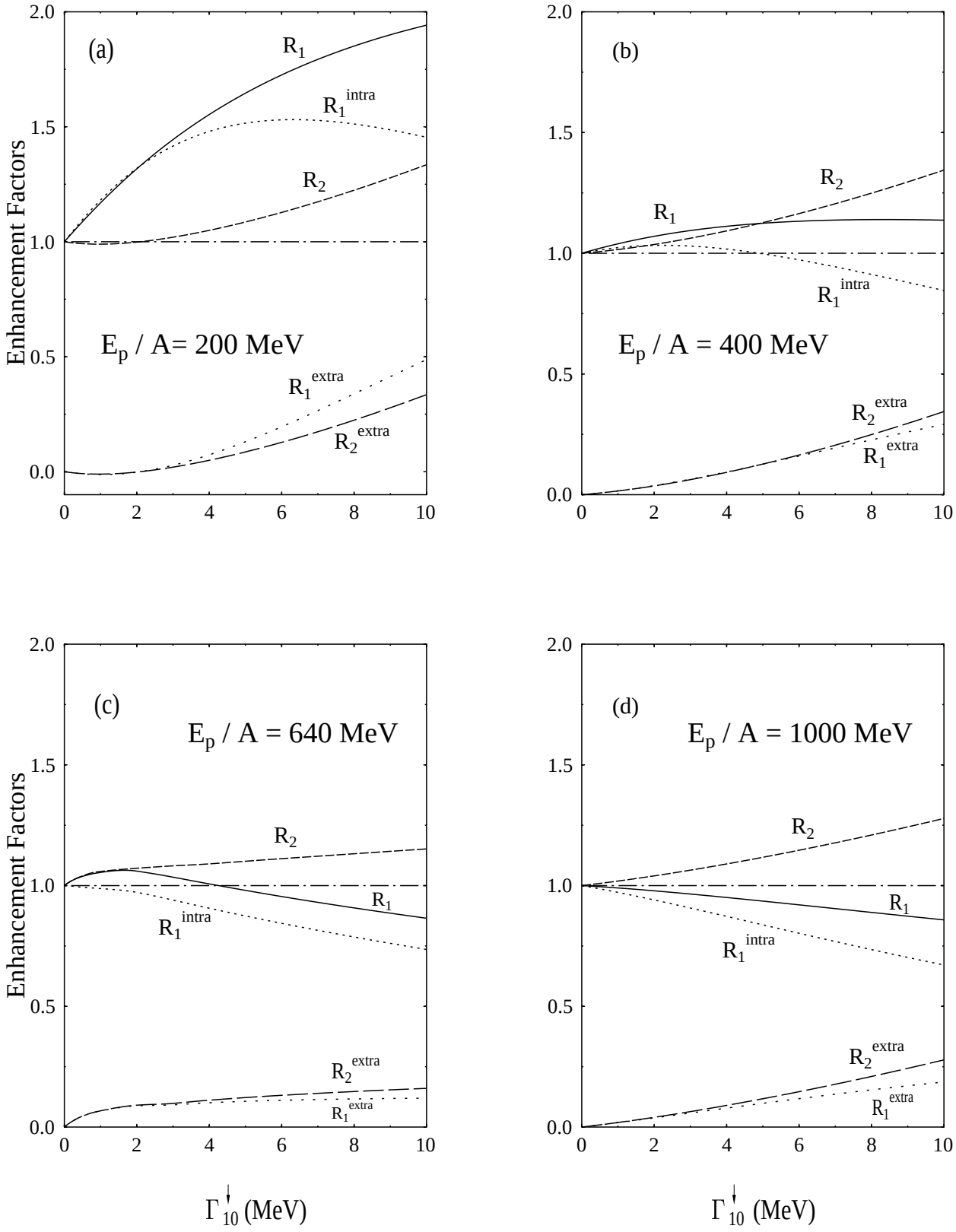
(a)
R_1
R_1^{intra}
R_2
E_p / A= 200 MeV
R_1^{extra}
R_2^{extra}
(b)
R_2
R_1
R_1^{intra}
E_p / A = 400 MeV
R_2^{extra}
R_1^{extra}
(c)
E_p / A = 640 MeV
R_2
R_1
R_1^{intra}
R_2^{extra}
R_1^{extra}
(d)
E_p / A = 1000 MeV
R_2
R_1
R_1^{intra}
R_2^{extra}
R_1^{extra}
Enhancement Factors
Enhancement Factors
0.0
0.5
1.0
1.5
2.0
0
2
4
6
8
10
$\Gamma_{10}^{\downarrow}$ (MeV)
$\Gamma_{10}^{\downarrow}$ (MeV)

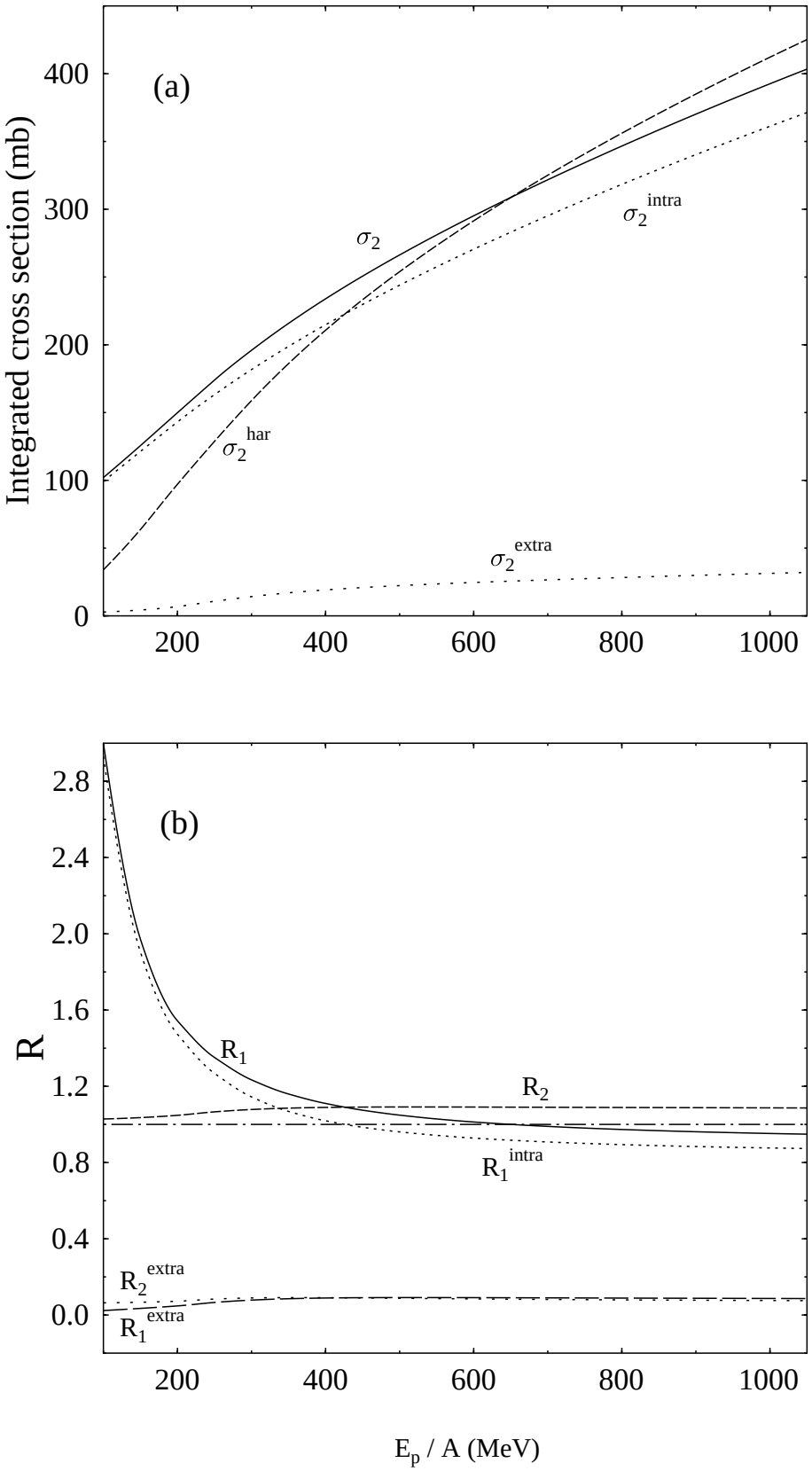
(a)
Integrated cross section (mb)
400
300
200
100
0
200
400
600
800
1000
σ_2
σ_2^{intra}
σ_2^{har}
σ_2^{extra}
(b)
R
2.8
2.4
2.0
1.6
1.2
0.8
0.4
0.0
R_1
R_2
R_1^{intra}
R_2^{extra}
R_1^{extra}
E_p / A (MeV)

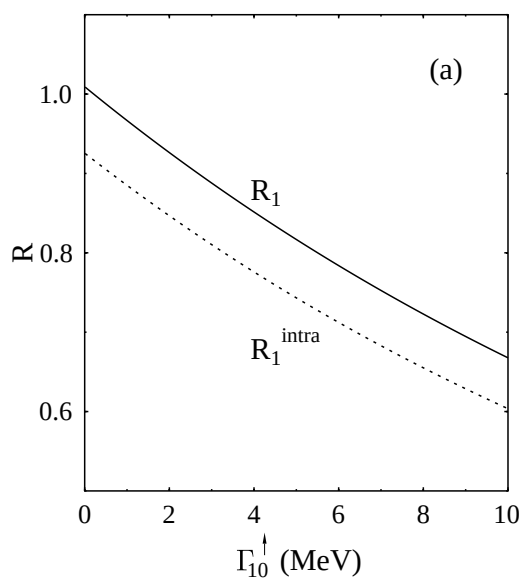
(a)
R
1.0
0.8
0.6
R_1
R_1^{intra}
0
2
4
6
8
10
$\Gamma_{10}^{\uparrow}$ (MeV)

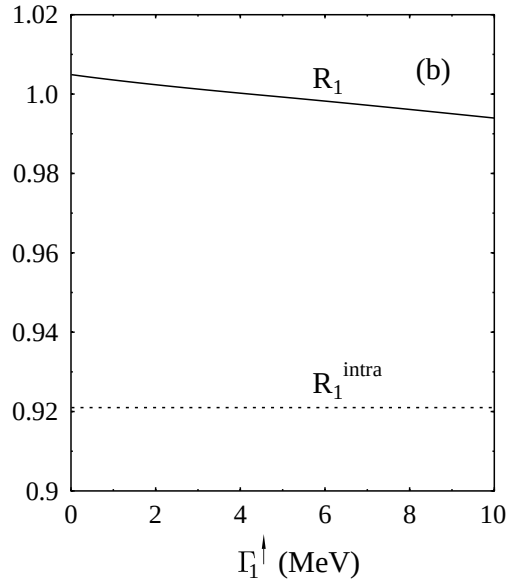
(b)
1.02
1.0
0.98
0.96
0.94
0.92
0.9
R_1
R_1^{intra}
0
2
4
6
8
10
$\Gamma_1^{\uparrow}$ (MeV)

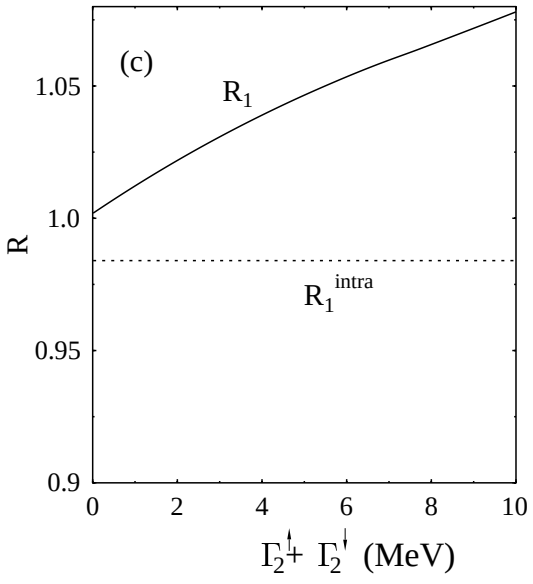
(c)
R
1.05
1.0
0.95
0.9
R_1
R_1^{intra}
0
2
4
6
8
10
$\Gamma_2^{\uparrow}$+ $\Gamma_2^{\downarrow}$ (MeV)

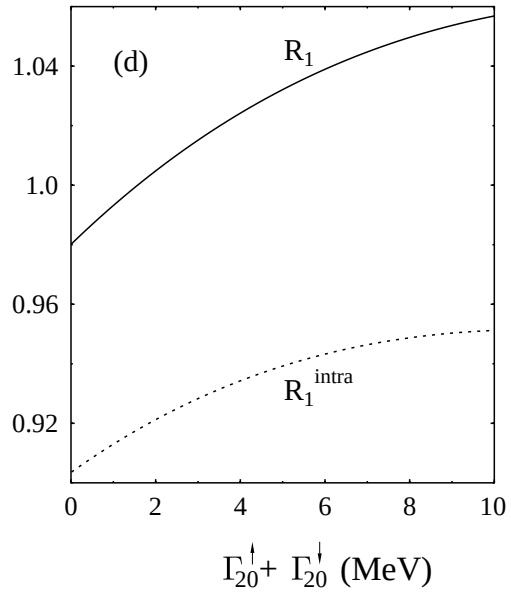
(d)
1.04
1.0
0.96
0.92
R_1
R_1^{intra}
0
2
4
6
8
10
$\Gamma_{20}^{\uparrow}$+ $\Gamma_{20}^{\downarrow}$ (MeV)

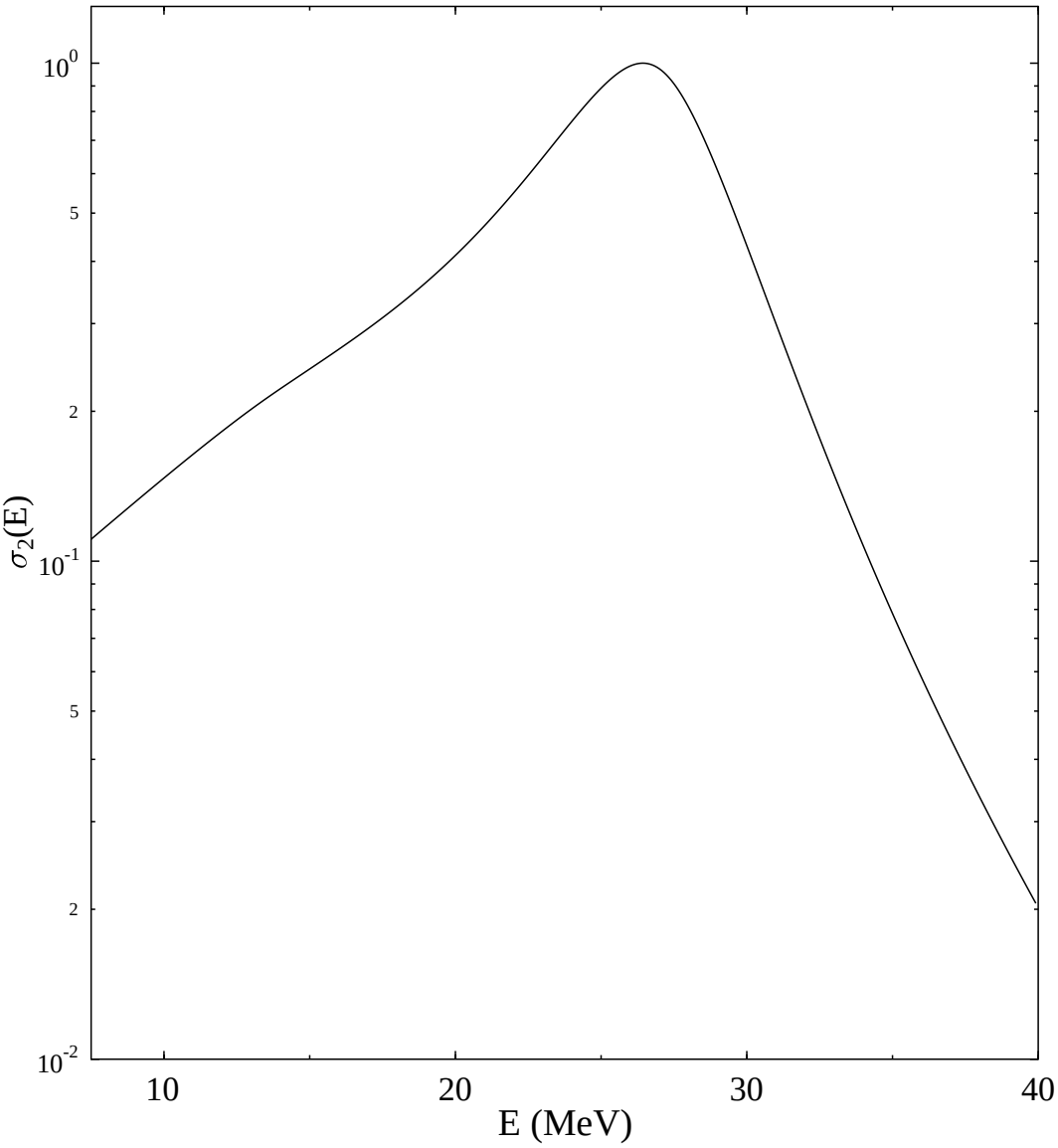
10^0
5
2
10^{-1}
5
2
10^{-2}
σ_2(E)
10
20
30
40
E (MeV)

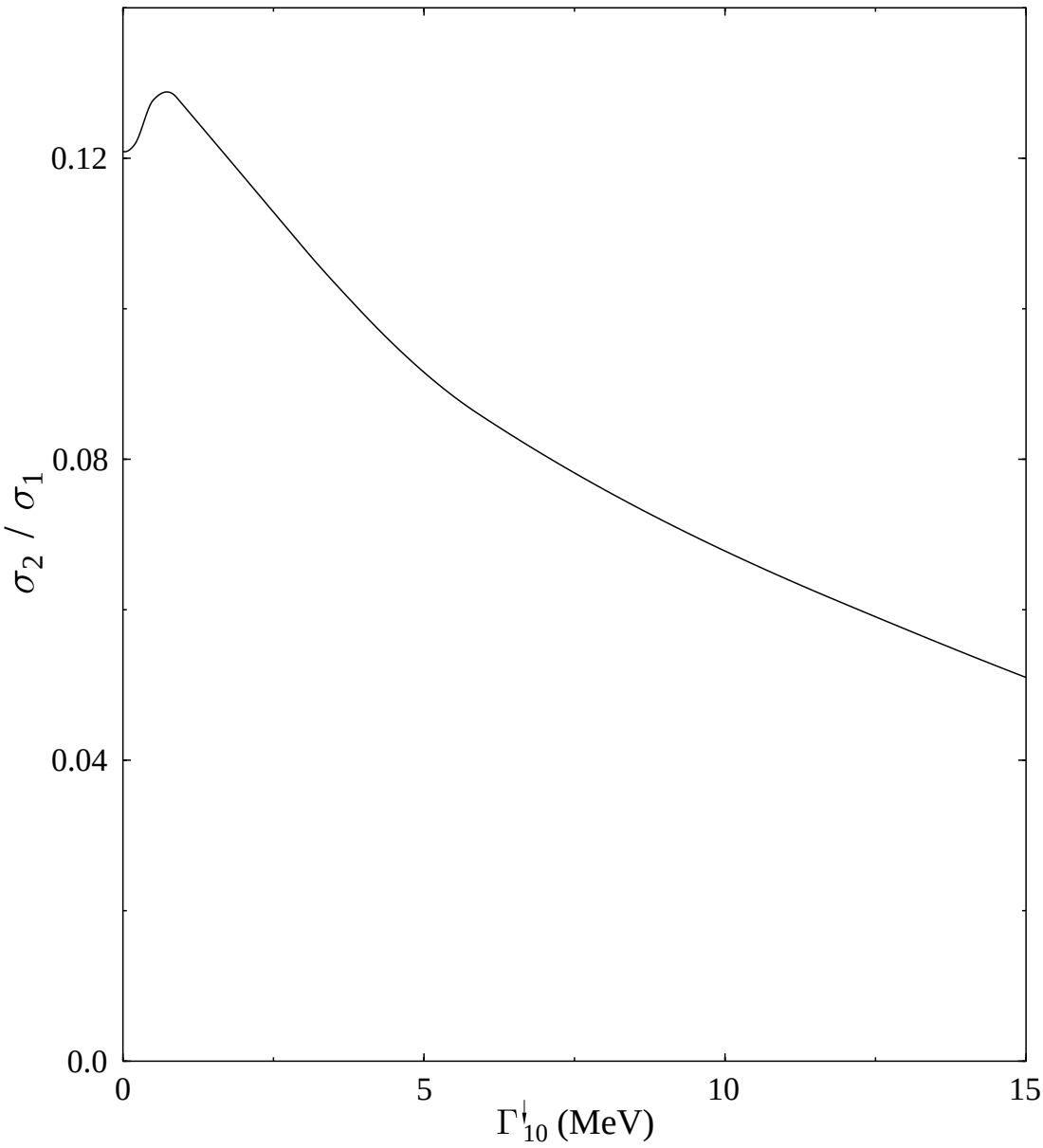
0.12
0.08
0.04
0.0
σ_2 / σ_1
0
5
10
15
$\Gamma^{\downarrow}_{10}$ (MeV)